

1 **The AAA+ ATPase ClpX Is Critical for Growth and Development of**

2 *Chlamydia trachomatis*

3  
4 Nicholas A. Wood<sup>1</sup>, Amanda M. Blocker<sup>2</sup>, Mohamed A. Seleem<sup>3</sup>, Martin Conda-Sheridan<sup>3</sup>,

5 Derek J. Fisher<sup>2</sup>, Scot P. Ouellette<sup>1#</sup>

6 <sup>1</sup>Department of Pathology and Microbiology, College of Medicine, University of Nebraska  
7 Medical Center, Omaha, NE

8 <sup>2</sup>School of Biological Sciences, Southern Illinois University Carbondale, Carbondale, IL

9 <sup>3</sup>Department of Pharmaceutical Sciences, College of Pharmacy, University of Nebraska Medical  
10 Center, Omaha, NE

11  
12  
13 Keywords: *Chlamydia*, differentiation, division, protein turnover, protein quality control, Clp  
14 protease

15  
16 Running Title: ClpX ATPase of *Chlamydia*

17  
18  
19 #Corresponding Author:

20 Department of Pathology and Microbiology, College of Medicine, University of Nebraska  
21 Medical Center, 985900 Nebraska Medical Center (DRC2 5022), Omaha, NE

22 Tel: +1-402-559-0763 Fax: +1-402-559-5900 Email: [scot.ouellette@unmc.edu](mailto:scot.ouellette@unmc.edu)

23

24 **Abstract:**

25 *Chlamydia trachomatis* (Ctr) is an obligate intracellular bacterium that undergoes a complex  
26 developmental cycle in which the bacterium differentiates between two functionally and  
27 morphologically distinct forms, each of which expresses its own specialized repertoire of  
28 proteins. The transitions between the infectious, non-dividing elementary body (EB) and the non-  
29 infectious, replicative reticulate body (RB) are not mediated by division events that re-distribute  
30 intracellular proteins. Rather, both primary (EB to RB) and secondary (RB to EB) differentiation  
31 require protein turnover. The Clp protease system is well conserved in bacteria and, minimally,  
32 relies on a serine protease subunit, ClpP, and a AAA+ ATPase, such as ClpX, that recognizes  
33 and unfolds substrates for ClpP degradation. In *Chlamydia*, *clpX* is encoded within an operon  
34 adjacent to *clpP2*. We present evidence that the chlamydial ClpX ortholog, and the co-  
35 transcribed ClpP2, play a key role in organism viability and development. We demonstrate here  
36 that chlamydial ClpX is a functional ATPase and forms the expected homohexamer *in vitro*.  
37 Overexpression of a ClpX mutant lacking ATPase activity had a limited impact on DNA  
38 replication or secondary differentiation but, nonetheless, reduced EB viability. Conversely, the  
39 overexpression of an inactive ClpP2 mutant significantly impacted later developmental cycle  
40 progression by reducing the overall number of organisms. Blocking *clpP2X* transcription using  
41 CRISPR interference led to a decrease in bacterial growth, which did not occur when the non-  
42 essential gene *incA* was targeted. Taken together, our data indicate that ClpX and the associated  
43 ClpP2 play a critical role in developmental cycle progression and differentiation.

44

45 **Words: 248/250**

46

47 **Importance**

48 *Chlamydia trachomatis* is the leading cause of infectious blindness globally and the most  
49 reported bacterial sexually transmitted infection both domestically and internationally. Given the  
50 economic burden, the lack of an approved vaccine, and the use of broad-spectrum antibiotics for  
51 treatment of infections, a further understanding of chlamydial growth and development is critical  
52 for the advancement of novel, targeted antibiotics. The Clp proteins comprise an important and  
53 conserved protease system in bacteria. Our work highlights the importance of the chlamydial Clp  
54 proteins to this clinically important bacterium. Additionally, our study implicates the Clp system  
55 playing an integral role in chlamydial developmental cycle progression, which may help  
56 establish models of how *Chlamydia* spp. and other bacteria progress through their respective  
57 developmental cycles. Our work also contributes to a growing body of Clp-specific research that  
58 underscores the importance and versatility of this system throughout bacterial evolution and  
59 further validates Clp-proteins as drug targets.

60

61 **Words: 150/150**

## 62 **Introduction**

63 *Chlamydia trachomatis* (Ctr) is the leading cause of both bacterial sexually transmitted  
64 infections (STIs) and infectious blindness worldwide (1, 2). When left untreated, STIs can result  
65 in chronic sequelae, including pelvic inflammatory disease, ectopic pregnancy, and tubal  
66 infertility. A better understanding of Ctr molecular processes may help reveal essential systems  
67 that can be leveraged for more targeted intervention strategies.

68 *Chlamydia* species are obligate intracellular bacterial pathogens that differentiate  
69 between distinct functional and morphological forms during the course of their developmental  
70 cycles (see (3) for a comprehensive review). The elementary body (EB) is small (~0.3  $\mu\text{m}$  in  
71 diameter), infectious, but non-dividing (4, 5). An EB attaches to a host cell and is internalized  
72 into a host membrane-derived vacuole that is rapidly modified into the inclusion (6-9). Within  
73 this inclusion, the EB undergoes primary differentiation into the larger (~1.0  $\mu\text{m}$  in diameter)  
74 reticulate body (RB). The RB is non-infectious but divides using a polarized budding mechanism  
75 (10) until secondary differentiation from an RB to an EB occurs. Studies over the years have  
76 extensively detailed the transcriptional and proteomic differences between EBs and RBs (e.g.  
77 (11-14)). Given that chlamydial differentiation is not preceded by an unequal division and  
78 redistribution of intracellular proteins, as occurs in other bacteria such as *Bacillus subtilis* (see  
79 (15) for review) or *Caulobacter crescentus* (16), and that EBs and RBs have distinct proteomes,  
80 we hypothesize that proteomic turnover plays an integral role in chlamydial differentiation.

81 Previously, our groups characterized the two ClpP paralogs of Ctr. We established that  
82 the core *clp* protease-associated genes are expressed in the mid-developmental cycle and that  
83 ClpP1 and ClpP2 likely perform unique roles in chlamydial physiology (17). In addition to the  
84 two ClpP paralogs, *C. trachomatis* encodes a ClpX homolog (18). ClpX is a Type I AAA+

85 (ATPase Associated with diverse cellular Activities) unfoldase that utilizes ATP hydrolysis to  
86 linearize protein substrates for either degradation by the ClpP protease or refolding (19, 20).  
87 Type I AAA+ ATPases encode Walker A and Walker B motifs, which are responsible for ATP  
88 binding and hydrolysis, respectively (21, 22). ClpX oligomerizes to form a homo-hexamer that  
89 then recognizes substrates through multiple different mechanisms (see (23) for a comprehensive  
90 review).

91         Here, we characterized the role of ClpX in chlamydial growth and development. Because  
92 *clpX* is encoded within an operon with *clpP2*, we investigated effects of overexpression and  
93 knockdown of both components. Ctr ClpX is highly conserved, possesses ATPase activity, and  
94 formed the expected homohexamer *in vitro*. Interestingly, overexpression of wild-type ClpX,  
95 ClpP2, and ClpP2X constructs in Ctr had little effect on bacterial growth, but overexpression of  
96 the inactive mutants (alone or in tandem) negatively impacted recoverable inclusion forming  
97 units (IFUs). However, the reduction in IFUs upon inactive ClpX overexpression resulted from  
98 non-functional EB generation while the IFU reduction upon inactive ClpP2 overexpression was  
99 the result of a block in developmental cycle progression. Our results indicate that chlamydial  
100 ClpX is a true ortholog of bacterial ClpX and that the ClpP2X system is integral to chlamydial  
101 growth and development.

102

103 **Words:**

**498/500**

104 **Results**

105 ***The chlamydial ClpX retains conserved motifs of, and exhibits predicted structural homology***

106 ***to, ClpX orthologs.*** To initiate our study, we first performed bioinformatic and *ab initio*

107 structural modeling analyses to determine whether the chlamydial ClpX (ClpX<sub>ctr</sub>) possesses the

108 expected conserved regions and motifs consistent with its proposed function as an AAA+

109 ATPase. Using multiple sequence alignment, we aligned ClpX<sub>ctr</sub> to ClpX orthologs and

110 annotated conserved motifs identified in other studies (Fig. 1a). ClpX<sub>ctr</sub> retains the N-terminal

111 metal binding domain (24, 25), the Walker A and B motifs for ATP binding and hydrolysis,

112 respectively (21, 23), the sensor motifs for recognition of nucleotide bound state (26), the RKH

113 motif and pore loops for substrate recognition (27-29) and unfolding (30, 31), the arginine finger

114 for inter-subunit sensing of nucleotide state in the ClpX hexamer (22, 32), and the IGF Loop for

115 interaction with ClpP (33, 34). Interestingly, the predicted secondary structure of ClpX<sub>ctr</sub> shows

116 few notable aberrations (see Discussion) from other prototypical bacterial ClpX orthologs and is

117 predicted to form the expected homohexamer by structural modeling (Fig. 1b, two subunits

118 removed for clarity). The spatial conservation of AAA+ and ClpX-specific motifs (colored in

119 Fig. 1b as in the multiple sequence alignment) indicates that the chlamydial ClpX likely

120 functions using a mechanism similar or identical to other ClpX orthologs. Taken together, these

121 *in silico* studies suggest ClpX<sub>ctr</sub> functions as a canonical AAA+ ATPase.

122

123 ***Chlamydial ClpX forms the expected homohexamer and possesses ATPase activity.*** To

124 determine the oligomeric state of ClpX<sub>ctr</sub> *in vitro*, we purified recombinant protein and analyzed

125 its migration by native PAGE. At the same time, we also constructed a Walker B ATPase mutant

126 (E187A) ClpX<sub>ctr</sub> as a control for biochemical studies. Following the incubation of 10 µg of wild-

127 type or mutant ClpX<sub>Ctrl</sub> for 20 minutes in a HEPES based buffer, we loaded the entire volume  
128 into a 4-20% gradient gel. We observed the ClpX<sub>Ctrl</sub> proteins migrating above the 242 kDa band  
129 of the molecular weight ladder, which is close to the expected hexameric size of 283 kDa (Fig.  
130 2a). We then sought to assess ATPase activity of recombinant wild-type and ATPase mutant  
131 ClpX<sub>Ctrl</sub> using the Biomol Green endpoint assay to measure free phosphate levels following ATP  
132 hydrolysis, which served as a proxy for ATPase activity. Indeed, ClpX<sub>Ctrl</sub> hydrolyzed ATP, while  
133 the inactive mutant isoform showed a significant defect in ATP hydrolysis (Fig. 2b). These data  
134 indicate that ClpX<sub>Ctrl</sub> (i) forms a homohexamer of the predicted size and (ii) possesses ATPase  
135 activity that is abrogated by a mutation in the Walker B motif.

136 We next tested whether wild-type and ATPase mutant ClpX<sub>Ctrl</sub> interact with each other  
137 using the Bacterial Adenylate Cyclase Two-Hybrid (BACTH) assay. This system is predicated  
138 on the reconstitution of adenylate cyclase activity by bringing two complementary fragments of  
139 the enzyme (T25 and T18) into close proximity by interacting proteins. Generation of cAMP by  
140 the reconstituted adenylate cyclase drives  $\beta$ -galactosidase production that can be measured  
141 qualitatively by the presence of blue colonies and growth on minimal medium (Fig. 2c) or  
142 quantitatively by measuring enzyme activity directly (Fig. 2d). We performed a series of  
143 pairwise interaction tests between the wild-type and mutant ClpX<sub>Ctrl</sub>. In each instance, we  
144 observed a positive interaction that was quantifiable and on par with the positive control (T25-  
145 Zip vs T18-Zip). We conclude from these data that the mutant isoform can interact with the wild-  
146 type isoform.

147  
148 ***Overexpression of inactive ClpX or inactive ClpP2 has both overlapping and independent***  
149 ***effects.*** We previously measured the effects of overexpression of both wild-type and catalytically

150 inactive ClpP2<sub>Ctrl</sub> on chlamydial growth and observed a modest reduction in growth at 24 hours  
151 post-infection (hpi) (17). We wanted to more carefully assess growth differences during the  
152 chlamydial developmental cycle in the presence of overexpressed wild-type and mutant ClpX<sub>Ctrl</sub>  
153 (and ClpX<sub>E187A</sub>), ClpP2<sub>Ctrl</sub> (and ClpP2<sub>S98A</sub>), or both together (ClpP2X<sub>Ctrl</sub>/ClpP2<sub>S98A</sub>ClpX<sub>E187A</sub>). To  
154 do this, we performed growth curves where we induced expression, or not, at 10 hpi and  
155 quantified growth at various timepoints after induction. Immunofluorescence analysis (IFA) of  
156 replicate treatments and quantification of recoverable inclusion forming units (IFUs; a proxy for  
157 EBs) revealed distinct effects upon overexpression of the individual components (Fig. 3a-c) as  
158 well as with the entire operon (Fig. 3d&e). We noted that overexpression of wild-type ClpP2<sub>Ctrl</sub>  
159 showed no appreciable effect at either 24 or 48 hpi (14 and 38 h pulses of induction,  
160 respectively), whereas overexpression of ClpP2<sub>S98A</sub> appeared to reduce the number of organisms  
161 present within the inclusion at 48 hpi but not 24 hpi (Fig. 3a). These observations correlated with  
162 the marked impact on EB production in the later time points of mutant ClpP2<sub>S98A</sub> but not wild-  
163 type ClpP2<sub>Ctrl</sub> overexpression (Fig. 3b). Conversely, inactive ClpX<sub>E187A</sub> overexpression resulted  
164 in smaller inclusions and a decrease in IFUs that was not observed for overexpression of the  
165 wild-type ClpX (Fig. 3a&c). These IFU recovery data suggest that Ctrl is more sensitive to  
166 ClpX<sub>Ctrl</sub> rather than ClpP2<sub>Ctrl</sub> disruption earlier in the developmental cycle, as the IFU reduction is  
167 exacerbated sooner with ClpX<sub>E187A</sub> overexpression (note the differences at 24hpi in Fig. 3b&c).  
168 As noted for the overexpression of individual wild-type isoforms, there was no significant impact  
169 on IFU recovery of overexpressing both wild-type ClpP2<sub>Ctrl</sub> and ClpX<sub>Ctrl</sub> in tandem. Consistent  
170 with the effects of overexpressing individual mutant isoforms, overexpression of the inactive  
171 ClpP2<sub>S98A</sub> and ClpX<sub>E187A</sub> isoforms in tandem showed an exacerbated phenotype throughout the  
172 developmental cycle as noted by both IFA and IFU assays (Fig. 3d&e). Importantly, the wild-



173 type chromosomal copies of ClpP2<sub>Cr</sub> and ClpX<sub>Cr</sub> continue to be expressed during these  
174 overexpression assays. Therefore, the true impact of overexpression of the mutant isoforms is  
175 likely underrepresented.

176

177 ***Functional disruption of ClpP2 blocks developmental cycle progression while ClpX disruption***

178 ***reduces EB viability.*** Given that the IFU assay only measures EB viability from a population and

179 not total bacterial numbers or differentiation status, we next wanted to address these nuances of

180 the chlamydial developmental cycle. We first measured genomic DNA as a proxy for total

181 number of bacteria (i.e. both RBs and EBs). From 24 hpi to 48 hpi, we observed a significant

182 drop in gDNA levels when ClpP2<sub>S98A</sub> was overexpressed alone or in the mutant operon

183 configuration (Fig. 4a). Conversely, overexpression of any wild-type protein had no significant

184 impact on DNA accumulation. Surprisingly, overexpression of the ClpX<sub>E187A</sub> also had no

185 significant impact on DNA levels in spite of the reduction in IFUs, suggesting total bacterial

186 numbers are unaffected. To determine differentiation status, we next assessed HctB levels, an

187 EB-specific gene product (35-37), by western blot as an indicator of secondary differentiation.

188 We normalized the integrated density of HctB to the integrated density of MOMP (major outer

189 membrane protein; present in both EBs and RBs) to ensure that we were comparing HctB levels

190 to the total number of bacteria. The relative HctB levels in samples where ClpP2<sub>S98A</sub> was

191 overexpressed were reduced substantially, suggesting the generation of fewer EBs and consistent

192 with IFU and genomic DNA data, whereas the other experimental conditions showed no changes

193 in relative HctB levels (Fig. 4b&c). These data suggest that overexpression of ClpX<sub>E187A</sub> does

194 not impact bacterial replication, as measured by gDNA levels, or RB-to-EB differentiation, as

195 measured by HctB levels. Therefore, we prepared samples for transmission electron microscopy

196 to examine at higher resolution the morphology of EBs and RBs from ClpP2<sub>S98A</sub> and ClpX<sub>E187A</sub>  
197 overexpressing strains. Consistent with other measured effects, ClpP2<sub>S98A</sub> overexpression  
198 resulted in smaller inclusions with fewer organisms (Suppl. Fig. 1a). In contrast, but consistent  
199 with its measured effects, ClpX<sub>E187A</sub> overexpression did not have an obvious effect on RB size or  
200 numbers *per se*; rather, more bacteria with unusual, multi-nucleate staining were observed, as  
201 indicated by the arrows (Suppl. Fig. 1b&d compared to uninduced in panel C). These abnormal  
202 forms may potentially be EBs with defects in chromosomal packaging or intermediate bodies  
203 that have not completed chromosomal condensation. Taken together with the IFU data (Fig. 3),  
204 these results suggest differential effects of overexpression of ClpP2<sub>S98A</sub> and ClpX<sub>E187A</sub> and, by  
205 inference, differential effects of these Clp components in the physiology of the organism.

206  
207 ***Knockdown of the clpP2X operon reduces recoverable progeny and results in reduced plasmid***  
208 ***retention.*** Overexpression of mutant isoforms of ClpP2<sub>Ctrl</sub> and/or ClpX<sub>Ctrl</sub> was sufficient to  
209 disrupt chlamydial development in the presence of endogenous ClpP2X<sub>Ctrl</sub>. However, we wanted  
210 to directly block the chromosomal copies by employing an improved version of the chlamydial  
211 CRISPR interference (CRISPRi) strategy previously described by us ((38) and Ouellette, *in*  
212 *prep*). CRISPRi relies on the inducible expression of a catalytically inactive Cas9 (dCas9) in  
213 combination with a guide RNA (gRNA) to block transcription at specific chromosomal sites  
214 (39). We transformed Ctrl L2 with vectors encoding the dCas9 and gRNAs targeting either the  
215 *clpP2X* or *incA* intergenic regions. IncA knockdown served as a control since *incA* is a non-  
216 essential gene (40). The CRISPRi transformants were used to infect HEP2 cells. When dCas9  
217 expression was induced at 10hpi, we observed a marked and rapid decrease in both *clpP2* and  
218 *clpX* transcript levels compared to the uninduced controls at 14hpi (Fig. 5a). Similar results were

219 observed when dCas9 expression was induced at 4hpi (data not shown). Importantly, we did not  
220 observe a decrease in transcript levels for *clpP1*, *euo*, and *omcB* (Suppl. Fig. 2; (12, 17, 41, 42)).  
221 As previously observed, IncA expression was uniformly blocked after dCas9 induction (Fig. 5b;  
222 (38)).

223 We next assayed chlamydial growth as measured by IFU recovery after inducible  
224 knockdown of the target genes. Expression of dCas9 was induced at 4hpi, and IFUs were  
225 harvested at 24 and 48hpi and titred on fresh cell monolayers in the presence of penicillin, the  
226 selection agent. When *clpP2X* expression was blocked at 4hpi, we noted a 5-fold decrease in  
227 penicillin-resistant (i.e. transformants containing the CRISPRi plasmid) IFUs at 24hpi but a more  
228 than 200-fold decrease at 48hpi (Fig. 5c). In performing these assays in the presence of  
229 penicillin, we observed numerous penicillin-sensitive organisms (i.e. aberrant RBs (43)) during  
230 the titration step, suggesting that the plasmid conferring resistance and encoding the CRISPRi  
231 system was being lost after induction of dCas9 expression. To test this, we quantified plasmid  
232 retention in the *clpP2X* knocked down samples and observed that blocking *clpP2X* expression  
233 resulted in ~75% plasmid loss at 24hpi and greater than 90% loss at 48hpi (Fig. 5d). These  
234 effects on IFUs and plasmid retention were not observed for *incA* knockdown (Fig. 5c and d).  
235 We note that *incA* knockdown did result in a reproducible, but transient, increase in IFUs at  
236 24hpi that returned to “normal” levels at 48hpi (Fig. 5c). The reasons for this are not clear.  
237 Nonetheless, we conclude from these data that blocking *clpP2X* expression is deleterious to  
238 *Chlamydia*, further highlighting its essentiality to this pathogen.

239  
240 ***Chemical disruption of ClpX function is detrimental to Ctr.*** Recently, ClpX-specific inhibitors  
241 were synthesized by the Sieber group and shown to interfere with ClpX ATPase activity. One

242 compound, identified as 334, was shown to have potent inhibitory activity towards ClpX  
243 whereas a derivative, 365, was inactive (44). We performed *ab initio* modelling and molecular  
244 dynamics simulations (45) to determine if these compounds could interact with an ADP-bound  
245 hexameric ClpX<sub>ctr</sub>. For 334, a high scoring model (-9.1 kcal/mol binding affinity, RMSD ~ 0)  
246 was predicted with the drug binding near to the ATP binding pocket, suggesting a mechanism of  
247 action where 334 likely occludes the ATPase site (Suppl. Fig. 3). Whether the effect stems from  
248 the blocking of ATP binding and subsequent destabilization of the complex, attenuation of  
249 ATPase function by preventing a conformational change of the complex, or steric hindrance of  
250 complex formation remains to be elucidated. Conversely, compound 365 bound outside of the  
251 ATP pocket with a much lower score (Suppl. Fig. 4).

252         Given the predicted effects of the ClpX inhibitors on the structure of ClpX<sub>ctr</sub>, we next  
253 leveraged these compounds to assess the effect of specifically disrupting ClpX<sub>ctr</sub> on chlamydial  
254 growth. We initiated our studies by treating or not *C. trachomatis* L2 infected HEp2 cells at 8 hpi  
255 with 25 µg of drug to target specifically RBs early in development. At 24 hpi, we either  
256 harvested and froze IFUs or replaced the medium containing either the drug or the vehicle  
257 control with fresh medium lacking these. The latter samples were harvested at 48 hpi and frozen,  
258 and then all collected samples were titred in the absence of drug treatment. Initial assessment of  
259 immunofluorescent controls showed a marked reduction in inclusion size after 334 treatment for  
260 both the 24 and 48 h timepoints (8-24h and 8-48h; Fig. 6a&b). This was accompanied by a  
261 severe decrease in recovery of IFUs to near the limit of detection (Fig. 6c). As expected, 365  
262 treatment had little effect on IFU recovery at 24 hpi but did reduce IFU numbers by a log  
263 following prolonged treatment (8-24h and 8-48h; Fig. 6a-c), supporting our docking simulation  
264 that showed lower affinity of 365 to ClpX<sub>ctr</sub>. Moreover, 334 had a bacteriostatic effect on *C.*

265 *trachomatis*, as removal at 24 hpi allowed for a substantial recovery in IFU counts (8-24h; Fig.  
266 6b&c).

267 We then sought to assess the importance of ClpX<sub>Ctrl</sub> function throughout the  
268 developmental cycle by treating either early, to target primary differentiation and inclusion  
269 establishment, or later, to target pre-formed EBs. Treatment with 334 from 0 to 8 hpi resulted in  
270 over a log reduction in recoverable IFUs, demonstrating the importance of ClpX<sub>Ctrl</sub> early during  
271 the developmental cycle (0-8h; Fig. 6a&c). Addition of 334 following 24 h of no treatment  
272 confirmed the bacteriostatic nature of the drug's effect on *C. trachomatis*, as the IFU titre failed  
273 to increase more than a log over the 24 h untreated samples (24-48h; Fig. 6b&c). Furthermore,  
274 the addition of 334 at 24 hpi suggests that preformed EB viability is not reduced following  
275 ClpX<sub>Ctrl</sub> inhibition. Whether this is due to the lack of drug permeability into the EBs or the  
276 reversibility of drug binding upon removal from the media is not clear. Overall, these data  
277 highlight the importance of ClpX<sub>Ctrl</sub> for chlamydial development.

278

## 279 **Discussion**

280 Given the unique roles and protein repertoires of the chlamydial developmental forms  
281 (EB/RB), we hypothesize that protein degradation is a critical factor in the differentiation process  
282 from one form to the other. The Clp system is highly conserved in both prokaryotic and  
283 eukaryotic systems where it has been described to perform important functions in both  
284 proteostasis and pathogenesis (46). The Clp system is nominally composed of a proteolytic  
285 subunit, ClpP, and a AAA+ ATPase that functions as an unfoldase to recognize substrates and  
286 feed them into the ClpP barrel for degradation (23). The work presented here expands our  
287 understanding of the chlamydial Clp protease system. Focusing on an initial characterization of

288 ClpX<sub>Cr</sub> and the role of the *clpP2X* operon, we demonstrated the importance of the Clp protease  
289 system during chlamydial growth and development.

290 Multiple lines of evidence support that the chlamydial ClpX is a *bona fide* AAA+  
291 ATPase. Firstly, multiple sequence alignment of ClpX<sub>Cr</sub> to orthologs of other bacteria revealed a  
292 perfect conservation of the motifs involved in nucleotide binding, ATP hydrolysis, and  
293 nucleotide-state sensing (Fig. 1) (47, 48). Secondly, homology-directed and *ab initio* modelling  
294 of ClpX<sub>Cr</sub> revealed that the spatial orientation of these domains is conserved as well (Fig. 1),  
295 though we acknowledge that structural studies are critical to drawing conclusions about ClpX<sub>Cr</sub>  
296 conformational states. Thirdly, ClpX<sub>Cr</sub> interacts with itself to form a homohexamer that  
297 possesses ATPase activity (Fig. 2). Importantly, this ATPase activity could be disrupted by a  
298 targeted mutation in the Walker B motif while having no effect on the oligomerization properties  
299 of the protein. Fourthly, a characterized ClpX inhibitor that disrupts its ATPase activity also  
300 disrupted the growth of *C. trachomatis* serovar L2 (Fig. 6). Finally, overexpression of a ClpX<sub>Cr</sub>  
301 ATPase mutant negatively impacted chlamydial growth and development (Figs. 3&4).

302 While we have characterized the ATPase function of ClpX<sub>Cr</sub> and its role in chlamydial  
303 growth, further work remains to determine whether this ClpX ortholog functions as an unfoldase.  
304 Nevertheless, our bioinformatics analysis supports this as ClpX<sub>Cr</sub> retains substrate recognition  
305 motifs, including both pore loops and the RKH motif for gripping and translocation of substrates  
306 (27-31). *Chlamydia* spp. also encode the tmRNA/ssrA tagging system for ribosomal rescue (18,  
307 49-52), which fits a model where ClpX<sub>Cr</sub> may play an integral role in turnover of tagged,  
308 partially translated peptides. Whether ClpX<sub>Cr</sub> can actually target SsrA-tagged substrates, and  
309 whether this tagging is for ribosomal rescue or more specific purposes (53, 54), remains to be

310 determined and is currently under investigation by our research group. A recent article, using an  
311 SsrA-tagged GFP, suggests this function of chlamydial ClpX may be conserved (55).

312 One unique feature of ClpX<sub>Ctr</sub> is the TSSTSSP link between the zinc binding domain  
313 (ZBD) and the rest of the protein. To date, the structure of the ZBD has not been crystallized  
314 with the rest of the protein due to its apparent disorder; yet, the ZBD of ClpX is important for its  
315 function in other bacteria to, for example, recognize specific substrates (24, 56, 57). We  
316 hypothesize that the TSSTSSP residues may serve a function in flexibility (58, 59) or extension  
317 of the N-terminus, which in turn may modulate its unfoldase/chaperone activity (60).  
318 Interestingly, an SP motif has been implicated in initiation of a Type I  $\beta$ -hairpin turn (61, 62),  
319 which may serve as a mechanism through which the ClpX<sub>Ctr</sub> N-terminus adopts a unique  
320 conformation to recognize uncharacterized adaptors. This linker may be phosphorylated, leading  
321 to a conformational switch of the intrinsically disordered N-terminus and enhancing the stability  
322 of the otherwise disordered ZBD. We are investigating the potential for a phosphorylation state  
323 to activate or attenuate ClpX<sub>Ctr</sub> function. We hypothesize that at least one of these situations aids  
324 in selectivity of ClpX<sub>Ctr</sub> *in vivo* activity, but we cannot rule out that any combination may  
325 function to yield multiple layers of control.

326 In *Chlamydia*, *clpX* is encoded in an operon with *clpP2*. Our data indicate that, not  
327 surprisingly, the ClpP2X<sub>Ctr</sub> system is highly regulated and essential. We previously demonstrated  
328 that unregulated ClpP<sub>Ctr</sub> activity, through the use of ClpP-activating antibiotics, is detrimental to  
329 *Chlamydia* (17). Here, we performed a systematic analysis of the effects of overexpression of  
330 wild-type or inactivated ClpP2X<sub>Ctr</sub> components. The overexpression of wild-type ClpP2<sub>Ctr</sub> and/or  
331 ClpX<sub>Ctr</sub> had no biologically or statistically significant effect on chlamydial growth that we could  
332 measure. However, overexpressing inactive ClpP2<sub>Ctr</sub>(S98A) and/or ClpX<sub>Ctr</sub>(E187A) resulted in

333 abrogation of chlamydial growth as measured by recovery of infectious progeny. Three  
334 observations should be noted. Firstly, the effect of inducibly-expressed proteins is measured in  
335 the presence of the endogenous chromosomally-expressed proteins. Therefore, it is likely that the  
336 inactive mutants would have even more dramatic effects on chlamydial growth in the absence of  
337 the wild-type chromosomal copy. For ClpX<sub>Ctrl</sub>, this is supported by the effects of the ClpX  
338 inhibitor on *Chlamydia* (Fig. 6), which effectively stopped chlamydial growth. Secondly, we  
339 demonstrated that the mutant proteins could interact *in vitro* with wild-type isoforms (Fig. 2).  
340 Therefore, we can infer that overexpression of the mutant proteins leads to their incorporation  
341 into the endogenous ClpX machinery to disrupt or impair its function. Thirdly, to our knowledge,  
342 ours is the first study to ectopically express two different tagged proteins in *Chlamydia*, showing  
343 both the feasibility of this approach and its potential utility to dissect chlamydial biology.

344 The overexpression of the catalytically inactive mutant Clp proteins in *Chlamydia*  
345 revealed potentially subtle differences in the role of each component in chlamydial growth and  
346 development. Surprisingly, we noted a roughly 50% reduction in detectable genomes (Fig. 4A)  
347 when ClpX<sub>Ctrl</sub>(E187A) was expressed whereas IFUs were reduced roughly 20-fold (Fig. 3). The  
348 production of EBs as measured by HctB levels did not appreciably change (Fig. 4b&c). This  
349 suggests that, while development is hindered, the drop in IFUs may be due to defective EB  
350 viability, infectivity, or inclusion establishment and not a defect in secondary differentiation *per*  
351 *se*. Support for this comes from electron microscopy images, which revealed unusual  
352 morphologies after overexpression of the mutant ClpX<sub>Ctrl</sub> isoform (Suppl. Fig. 1). Conversely, for  
353 ClpP2<sub>Ctrl</sub>(S98A) overexpression, the substantial IFU decrease coupled with a sharp drop in gDNA  
354 levels indicate that ClpP2<sub>Ctrl</sub> plays a role in developmental cycle progression. HctB levels are also  
355 significantly reduced, which is consistent with the lack of EB generation. Taken together, these



356 data may indicate that ClpP2<sub>Cr</sub> is integral to developmental cycle progression or differentiation  
357 and that its function is tightly regulated. We cannot, however, exclude that secondary  
358 differentiation is directly affected due to the fact that total organism numbers are severely  
359 reduced. Rather, our proposed model suggests that ClpP2<sub>Cr</sub> disruption may affect both factors by  
360 a mechanism that we are currently working to identify. Conversely, ClpX<sub>Cr</sub> may serve a more  
361 prominent ClpP2<sub>Cr</sub>-independent function in differentiation of the organism (Suppl. Fig. 5).

362 We successfully generated chlamydial transformants with an inducible knockdown  
363 system to repress ClpP2X<sub>Cr</sub> expression. To date, this study is the first of its kind in *Chlamydia* to  
364 knock down genes that are essential, highlighting the utility of CRISPRi in studies of chlamydial  
365 biology while providing insight into possible ClpP2X<sub>Cr</sub> function. Notably, we observed a large  
366 decrease in IFU production coupled with an increase in plasmid loss after inhibition of *clpP2X*  
367 expression (Fig. 5). These effects were not observed when targeting a non-essential gene. Of  
368 note, penicillin does not kill chlamydiae but blocks cell division (63, 64), which keeps the  
369 organism transcriptionally in an RB-like state (65). This suggests that knocking down an  
370 essential gene(s) puts selective pressure on the chlamydiae to lose the plasmid encoding the  
371 CRISPRi system. This has important ramifications for long-term experiments and functional  
372 analyses. Nevertheless, the CRISPRi system represents a significant advance for our ability to  
373 study essential systems in this obligate intracellular bacterium.

374 In conclusion, we have demonstrated the importance of the ClpP2X<sub>Cr</sub> system to  
375 chlamydial development, but many questions remain unanswered. These include why ClpP2<sub>Cr</sub>  
376 and ClpX<sub>Cr</sub> may serve independent purposes and what substrates this system may be targeting.  
377 Additionally, we need to identify any cofactors, chaperones, adaptor proteins, or a lack thereof  
378 that may be pertinent to this system. We plan to dissect the structural motifs of ClpP2<sub>Cr</sub> and

379 ClpX<sub>Ctr</sub> to determine if any of the noted differences from other bacterial Clp proteins may alter  
380 activity, which may aid in our goal of further functional assessment. Finally, we need to continue  
381 experimentation to address our overarching hypothesis that protein turnover plays a role in  
382 chlamydial differentiation, and that the Clp system is a significant aspect of this model. Overall,  
383 we conclude that the chlamydial ClpP2X<sub>Ctr</sub> system is critical to the development of these  
384 obligate intracellular bacteria.

385 **Materials and Methods:**

386 **Strains and Cell Culture:** The human epithelial cell line HEP2 was used for the overexpression  
387 assays, gDNA and protein extractions, and antibiotic studies. McCoy mouse fibroblasts were  
388 used for chlamydial transformation, and human epithelial HeLa cells were used for plaque  
389 purification. All of these cell lines were passaged routinely in Dulbecco's Modified Eagle's  
390 Medium (DMEM, Gibco/ThermoFisher) and 10% FBS (Sigma; St. Louis, MO) and verified to  
391 be mycoplasma-free using LookOut<sup>®</sup> Mycoplasma PCR Detection Kit (Sigma). Density gradient  
392 purified *Chlamydia trachomatis* L2/434/Bu (ATCC VR902B) EBs were used for the antibiotic  
393 studies. *C. trachomatis* serovar L2 EBs (25667R) naturally lacking the endogenous plasmid were  
394 prepared and used for transformation [see (66)].

395

396 **Bioinformatics Analysis:** Gene sequences of *Chlamydia trachomatis* were obtained from  
397 STDGen database (<http://stdgen.northwestern.edu>) or KEGG Genome Browser (67-69). RefSeq  
398 protein sequences from *Escherichia coli*, *Bacillus subtilis*, *Mycobacterium tuberculosis*,  
399 *Staphylococcus aureus*, and *Pseudomonas aeruginosa* were acquired from the NCBI protein  
400 database (<https://www.ncbi.nlm.nih.gov/guide/proteins/>). ClpX pairwise protein alignments to  
401 find sequence identity were performed using NCBI Protein BLAST function  
402 (<https://blast.ncbi.nlm.nih.gov/Blast.cgi>) (70). Multiple sequence alignments were performed  
403 using Clustal Omega (71) with default settings and were presented using Jalview Version 2 (72).  
404 PDB files for predicted monomeric 3D structures were acquired from the Phyre2 website  
405 (<http://www.sbg.bio.ic.ac.uk/phyre2/html/page.cgi?id=index>) (73). Complexes were modelled  
406 using SWISS-MODEL available on the ExPASy server (74-77). Protein models and model  
407 alignments were rendered using the UCSF Chimera package from the Computer Graphics

408 Laboratory, University of California, San Francisco (supported by NIH P41 RR-01081) (78).  
409 Docking analyses were performed with AutoDock Vina using the default parameter settings (45).  
410 Molecules were prepped using Dunbrack rotamer libraries (79, 80) to replace incomplete side  
411 chains and ANTECHAMBER for charge assignment and topology generation (81).

412  
413 **Plasmid Construction:** A full list of the primers and plasmids used is included in the  
414 supplementary material. The Gateway® recombination system of cloning was used for plasmids  
415 for the Bacterial Adenylate Cyclase Two-Hybrid (BACTH) system (82). The genes were  
416 amplified from *Chlamydia trachomatis* L2 genomic DNA with added *attB* recombination sites.  
417 The PCR products were then incubated with a pDONR<sup>TM</sup>221 entry vector (containing *attP*  
418 recombination sites) in the presence of BP Clonase II (Invitrogen) to insert the gene via flanking  
419 *attP* recombination sites and remove the *ccdB* insert, resulting in an entry vector containing the  
420 gene of interest flanked by *attL* sites. These constructs were transformed into DH5 $\alpha$  chemically  
421 competent *E. coli* and plated onto kanamycin-containing LB agar. Plasmid was isolated and used  
422 for the LR reaction into one of three destination vectors (pST25-DEST, pSNT25-DEST, or  
423 pUT18C-DEST). The same entry vector for any given gene was used for all three LR reactions  
424 to insert into the destination vector. Entry vector and destination were incubated in a 1:1 ratio.  
425 DH5 $\alpha$  *E. coli* were transformed with 2  $\mu$ L of the reaction mix. Purified plasmid from an  
426 individual colony was sequence verified prior to use in the BACTH assay (see below).

427       Constructs for chlamydial transformation were created using the HiFi Cloning (New  
428 England Biolabs) protocol. Primers were designed to add a poly-Histidine (6xHis) tag to the  
429 gene of interest with the overlap to insert into the shuttle vector. Primers were generated using  
430 the NEBuilder® assembly tool available from New England BioLabs (<http://nebuilder.neb.com>).

431 The backbone used was the pTLR2 derivative of the pASK plasmid (83). For the CRISPRi  
432 plasmid, the *S. aureus* dCas9 was PCR amplified from pX603-AAV-CMV::NLS-  
433 dSaCas9(D10A,N580A)-NLS-3xHA-bGHpA (a gift from Dr. F. Zhang; Addgene plasmid #  
434 61594 (39)) and inserted into a derivative of pBOMB4-Tet::L2 (kind gift of Dr. T. Hackstadt,  
435 NIH; (84)) modified to weaken its ribosome binding site (Ouellette *in prep*). The gRNA cassettes  
436 were designed as previously described (38)), ordered as gBlock fragments from IDTDNA  
437 (Coralville, IA), and inserted into the BamHI site of the pBOMB4-Tet derivative encoding  
438 *Sa\_dCas9* to produce, for example, the plasmid pBOMBLCRia::L2 (*clpP2X*). HiFi reactions  
439 were assembled according to the manufacturer's protocol. The reaction was transformed into  
440 DH10 $\beta$  *E. coli*, and isolated plasmid was verified by restriction enzyme digest and sequencing by  
441 Eurofins Genomics. Sequence verified plasmids were transformed into *dam-/dcm-* *E. coli* (New  
442 England BioLabs) to produce demethylated plasmid, which was verified as described earlier  
443 prior to transformation into *C. trachomatis* (see below).

444 For mutation of ClpX Walker B motif, Q5 mutagenesis (New England BioLabs) was  
445 used. Primers were designed encoding the E187A mutation for PCR linearization of the plasmid.  
446 ClpX BACTH constructs were used as a template for the PCR amplification, and plasmids were  
447 re-circularized by KLD reaction. The resulting reactions were transformed into DH5 $\alpha$  *E. coli* for  
448 plasmid production. Plasmids were isolated, and mutations were verified by Sanger sequencing  
449 (Eurofins Genomics) prior to use in the BACTH system. These plasmids also served as template  
450 for the PCR reactions to produce PCR products for insertion of the mutant *clpX* gene into the  
451 pTLR2 plasmid.

452 Strains created or used in this study are listed in the supplementary material. Transformed  
453 *E. coli* strains were maintained on LB agar plates, with antibiotics as necessary. To extract

454 chlamydial genomic DNA, EBs were subjected to heat and proteinase K treatment prior to  
455 phenol:chloroform extraction (85). Sodium hydroxide lysis was utilized for the extraction of *E.*  
456 *coli* genomic DNA. For cloning into the pLATE31 plasmid, the aLICator LIC Cloning and  
457 Expression Kit 3 (Thermo Scientific) was used according to the manufacturer's specifications.  
458 Plasmids were first cloned into DH5 $\alpha$  *E. coli* for plasmid propagation. Transformants were  
459 screened for inserts using colony PCR with Fermentas Master Mix (Thermo Scientific) and  
460 positive clones were grown for plasmid isolation (GeneJet Plasmid Miniprep Kit, Thermo  
461 Scientific). Sequence verified plasmids were then transformed into BL21(DE3)  $\Delta$ *clpPAX* *E. coli*  
462 (55) for subsequent protein purification.

463

464 ***Purification of Recombinant ClpX:*** His-tagged Ctr ClpX and Ctr ClpX<sub>(E187A)</sub> were purified from  
465 500 mL cultures of BL21(DE3)  $\Delta$ *clpPAX* *E. coli* transformed with the respective plasmid based  
466 on the protocol described in (17). Samples were induced with 0.5 mM IPTG and incubated with  
467 shaking for 20 hours at 18°C. Cultures were pelleted and frozen at -80°C prior to purifications.  
468 Samples were suspended in buffer A (25 mM Tris Base [pH 7.5], 300 mM NaCl, and 10 mM  
469 Imidazole), sonicated, bound to HisPur Cobalt Resin (Thermo Scientific), and washed in buffer  
470 A Proteins were eluted from the resin using buffer B (25 mM Tris Base [pH 7.5], 300 mM NaCl,  
471 and 300 mM Imidazole). Buffer exchange for ATPase assay buffer (25 mM HEPES [pH 7.2],  
472 200 mM KCl, 20 mM MgCl<sub>2</sub>, and 10% glycerol) was performed using a Millipore Amicon Ultra  
473 15 filtration units (3 kDa cut-off). ClpX proteins were quantified using the Bio-Rad Protein  
474 assay, assessed for purity on 10% SDS-PAGE gels with Coomassie staining (Suppl. Fig. 6), and  
475 identified using anti-His-tag western blot. Blotting was performed using a mouse monoclonal

476 anti-6x His antibody (1:1000; Millipore HIS.H8) and a goat anti-mouse IgG HRP conjugated  
477 secondary antibody (1:2000). Protein samples were aliquoted and stored at -80°C.

478

479 ***In Vitro Analysis of ClpX Homo-Oligomerization:*** 10 µg of purified protein was incubated at  
480 for 20 minutes at 37°C in oligomerization buffer (25 mM Tris Base [pH 7.5], 5 mM KCl, 5 mM  
481 MgCl<sub>2</sub>, 1 mM DTT, and 1% glycerol) prior to mixing with a 5x native sample buffer (5 mM Tris  
482 [pH 6.8], 38 mM glycine, 0.06% bromophenol blue). Assays were analyzed on a BioRad  
483 MiniProtean 4-20% gradient gel for Native-PAGE. Gels were assessed using Coomassie  
484 staining.

485

486 ***Assessment of ClpX ATPase activity in vitro.***

487 A 49 µl reaction containing 1.5 µg of recombinant wild-type ClpX or ClpX<sub>(E187A)</sub> in ATPase  
488 assay buffer (see above) was preincubated for 10 minutes at room temperature without ATP.  
489 Next, ATP dissolved in ATPase assay buffer was added to 1 mM giving a final volume of 50 µl,  
490 and the reaction was incubated at 30° C for 2 hours. After the 2 hours, 200 µl of BIOMOL Green  
491 reagent (Enzo Life Sciences) was added and incubated at room temperature for 20 minutes. The  
492 absorbance of each reaction was then measured at 620nm using a BioTek Synergy HT plate  
493 reader. Reactions were performed in duplicate at least four times with at least two independent  
494 protein preparations.

495

496 ***Determining Protein-Protein Interactions with the BACTH System:*** The Bacterial Adenylate  
497 Cyclase Two-Hybrid (BACTH) assay was utilized to test interactions between wild-type and  
498 mutant ClpX (86). The genes of interest are translationally fused to one of either subunit,

499 denoted as T18 and T25, of the *B. pertussis* adenylate cyclase toxin, which can complement  
500 adenylate cyclase deficient ( $\Delta cya$ ) DHT1 *E. coli*. Wild-type and mutant *clpX* genes cloned into  
501 one of the pST25, pSNT25, or pUT18C Gateway<sup>®</sup> vectors was tested for both homotypic and  
502 heterotypic interactions (9, 82). Plasmids from each background were co-transformed into  
503 chemically competent DHT1 *E. coli*, which were plated on a double antibiotic minimal M63  
504 medium selection plate supplemented with 0.5 mM IPTG for induction of the protein, 40  $\mu$ g/mL  
505 Xgal, 0.04% casein hydrolysate, and 0.2% maltose. Leucine zipper motifs were used for controls  
506 in pKT25 and pUT18C backgrounds on the appropriate antibiotic selection plates because these  
507 have been previously shown to interact (87). Blue colonies, indicative of positive interaction,  
508 were screened using the  $\beta$ -galactosidase assay. Random positive colonies were selected and  
509 grown in M63 minimal media with the appropriate antibiotics. 0.1% SDS and chloroform were  
510 used to permeabilize the bacteria prior to addition of 0.1% o-nitrophenol- $\beta$ -galactoside (ONPG).  
511 1 M NaHCO<sub>3</sub> was used to stop the reaction after precisely 20 minutes of incubation at room  
512 temperature. Absorbance at the 405 nm wavelength was recorded and normalized to bacterial  
513 growth (OD<sub>600</sub>), dilution factor, and time (in minutes) of incubation prior to stopping the  
514 reaction. Totals were reported in relative units (RU) of  $\beta$ -galactosidase activity.

515

516 ***Chlamydial Transformation:*** The protocol followed was a modification of the method  
517 developed by Mueller and Fields (88) and as previously described (17). For transformation, 10<sup>6</sup>  
518 *C. trachomatis* serovar L2 EBs (25667R) naturally lacking the endogenous plasmid were  
519 incubated with 2  $\mu$ g of unmethylated plasmid in a volume of 50  $\mu$ L CaCl<sub>2</sub> at room temperature  
520 for 30 minutes. Reaction volume was sufficient for one well of a six well plate of McCoy mouse  
521 fibroblasts. Transformants were mixed with 1 mL of HBSS and added to 1 mL of HBSS in a six



522 well plate. The plates were centrifuged at room temperature for 15 minutes, 400 xg. The plate  
523 was then incubated at 37° C for 15 minutes. After incubation, the HBSS was aspirated and  
524 replaced with antibiotic-free DMEM+10% FBS. 8 hours post-infection, the media was replaced  
525 with DMEM containing 1 µg/mL cycloheximide and 1 U/mL penicillin. Cells infected with  
526 transformants were passaged every 48 hours until a population of penicillin resistant bacteria was  
527 established. EBs were harvested and frozen in sucrose/phosphate (2SP; (66)) solution at -80° C.

528

529 ***Determining the Effect of Overexpression of Wild-Type and Mutant Clp Proteins via***  
530 ***Immunofluorescence and Inclusion Forming Unit Analysis: C. trachomatis*** transformants  
531 containing plasmids encoding the 6xHis-tagged protein of interest were used to infect a confluent  
532 monolayer of HEp2 cells. Penicillin treatment was maintained throughout the duration of the  
533 infection. At 10 hpi, samples were induced or not with 10 nM anhydrotetracycline (aTc). At the  
534 given timepoints, three wells of a 24 well plate were scraped in 2SP, vortexed with three 1 mm  
535 glass beads, and frozen at -80° C. At the same timepoint, a coverslip was fixed in 3.25%  
536 formaldehyde and 0.025% glutaraldehyde for two minutes, followed by permeabilization with  
537 cold 90% methanol for one minute. Coverslips were labeled with primary goat anti-major outer  
538 membrane protein (MOMP; Meridian, Cincinnati, OH), rabbit anti-6xHis (Abcam, Cambridge,  
539 MA), and DAPI. Appropriate donkey secondary antibodies were used (Invitrogen, Carlsbad,  
540 CA). Images were acquired on an Axio ImagerZ.2 equipped with Apotome.2 optical sectioning  
541 hardware and X-Cite Series 120PC illumination lamp. Frozen IFU samples were titrated onto a  
542 fresh monolayer of HEp2s without antibiotics. At 24 hpi, samples were fixed with methanol for  
543 10 minutes, stained for MOMP, and enumerated.

544

545 ***Genomic DNA Isolation and qPCR Enumeration of Genomic Equivalents:*** At 24 or 48 hpi,  
546 one well of a six well plate was scraped into the media overlay and pelleted at 17000 xg, 4° C for  
547 15 minutes. Each sample was resuspended in 500 µL of cold PBS, frozen three times at -80° C,  
548 and processed using the Qiagen DNeasy Blood and Tissue Kit according to the manufacturer's  
549 specifications. DNA concentrations were assessed using a spectrophotometer prior to dilution  
550 down to 5 ng/µL. 5 µL of the resulting dilution was used for a 25 µL qPCR reaction volume  
551 using SYBR<sup>®</sup> Green PCR Master Mix (Applied Biosystems). Each reaction was performed in  
552 triplicate. A standard curve using Ctr L2 genomic DNA was generated for interpolation of  
553 sample Ct values. This experiment was performed three times for three biological replicates.

554

555 ***Analysis of HctB Levels Upon Clp Overexpression:*** At 24 or 48 hpi, one well of a six well plate  
556 per test condition was rinsed twice with HBSS. To lyse the cells, 500 µL of denaturing lysis  
557 buffer (8 M Urea, 10 mM Tris, 2.5% 2-mercaptoethanol, 1% SDS) was added to each well and  
558 incubated for 15 minutes at room temperature. 300 units of Universal Nuclease (Pierce) per mL  
559 of lysis buffer was added immediately prior to addition to the wells. Following incubation,  
560 samples were centrifuged at 17000 xg, 4° C for 15 minutes to remove any insoluble material.  
561 Samples were quantitated using the EZQ Protein Quantitation Kit (Pierce). 50 µg of each sample  
562 was run in a 4-20% gradient SDS-PAGE gel (BioRad) and transferred to a PVDF 0.45 µm pore  
563 size membrane for 1 h at 300 mA. The membrane was probed using goat anti-MOMP (Meridian)  
564 and rabbit anti-HctB (generously provided by Dr. T. Hackstadt, NIH) primary antibodies  
565 followed by staining with donkey anti-goat 680 and donkey anti-rabbit 800 (LI-COR) secondary  
566 antibodies. The membrane was imaged on an Azure c600 imaging system. The channels were  
567 gray-scaled and equally contrast corrected, and the resulting images were used for integrated

568 density measurement with FIJI software (89). To assess relative HctB levels, the HctB integrated  
569 density of each sample was normalized to its respective MOMP integrated density to avoid bias  
570 due to lower overall organism numbers. The ratios were then used to compare induced versus  
571 uninduced relative HctB levels. These experiments were performed three times for a total of  
572 three biological replicates.

573

574 ***Transmission electron microscopy (TEM) assessment of the effect of inactive Clp***  
575 ***overexpression.*** Samples were infected and induced as previously discussed (see above). At 48  
576 hpi, samples were fixed using 2% Glutaraldehyde, 2% Formaldehyde in 0.1M Sorensen's  
577 phosphate buffer, pH 7.2. Samples were then stained post-fixation in 1% Osmium Tetroxide in  
578 water for 1 hour. Samples were dehydrated in an Ethanol series 50%, 70%, 90%, 95%, 100% 3  
579 changes of 100%, all steps 15 minutes each and were then soaked in Propylene Oxide 100% 3  
580 changes for 15 minutes each. Samples were left overnight in a fume hood in a 1:1 mixture of  
581 Propylene Oxide and Embed 812. The following day the samples were placed in molds with  
582 fresh Embed 812 and polymerized overnight in an oven set at 65° C. Blocks were thin sectioned  
583 90 nanometers thick on a Leica UC6 Ultramicrotome using a Diatome diamond knife. Sections  
584 were placed on uncoated 200 mesh copper grids and stained with 2% Uranyl Acetate and  
585 Reynold's Lead Citrate. Sections were examined on a FEI Tecnai G2 TEM operated at 80Kv.

586

587 ***Confirmation of clpP2X and incA knockdown.*** Briefly, two wells of a six-well plate per  
588 condition were infected with pBOMBLCRia-clpP2X transformed CtrL2 at an MOI of 0.8. At  
589 either four or ten hpi, samples were or were not induced with 10 nM aTc. At each given  
590 timepoint, total RNA was collected using Trizol reagent (Invitrogen) and was extracted with

591 chloroform as described previously (17, 85, 90-92). The aqueous layer was precipitated using  
592 isopropanol, as per the manufacturer's instructions. Samples were DNase treated using the  
593 TURBO DNA-free kit (Ambion), and 1  $\mu$ g of the resulting RNA was reverse transcribed using  
594 SuperScript III reverse transcriptase (Invitrogen). Equal volumes of cDNA were loaded for each  
595 qPCR reaction. To extract genomic DNA, one well per condition was harvested and processed  
596 using the DNeasy blood and tissue kit (Qiagen) according to the manufacturer's instructions as  
597 noted above. Samples were diluted to 5 ng/ $\mu$ L, and 5  $\mu$ L of the resulting dilution was used per  
598 qPCR reaction. cDNA and gDNA samples were quantified using 25  $\mu$ L reactions with 2x SYBR  
599 PowerUP Green Master Mix (Invitrogen) analyzed on a QuantStudio 3 (Applied Biosystems)  
600 thermal cycler using the standard cycling conditions. A standard curve using purified wild-type  
601 CtrL2 genomic DNA was generated for sample quantification. Data are displayed as the ratio of  
602 cDNA to gDNA normalized to the 10h uninduced sample. For *incA* knockdown, HEp2 cells  
603 were infected with the pBOMBLCRia-*incA* transformant, induced with 10 nM aTc as above, and  
604 fixed at 24hpi with methanol. Cells were labeled with primary guinea pig anti-major outer  
605 membrane protein (MOMP; kind gift of Dr. E. Rucks, UNMC), rabbit anti-Sa\_dCas9 (Abcam,  
606 Cambridge, MA), sheep anti-IncA (Dr. E. Rucks), and DAPI. Appropriate donkey secondary  
607 antibodies were used (Invitrogen). Images were acquired on an Axio ImagerZ.2 equipped with  
608 Apotome.2 optical sectioning hardware and X-Cite Series 120PC illumination lamp.

609

610 ***Determination of the effect of clpP2X knockdown on Ctr.*** 24-well plates of HEp2 cells were  
611 infected at an MOI of 0.8 with either pBOMBLCRia-*clpP2X* or pBOMBLCRia-*incA*  
612 transformed into CtrL2. Samples were induced or not at 4 hpi and were harvested, fixed, and  
613 titered as previously described. Each titration was fixed using 4% formaldehyde and 0.025%

614 glutaraldehyde to preserve GFP fluorescence. IFU counts of GFP positive inclusions are  
615 displayed as a percentage of the uninduced sample at the given timepoint. Plasmid retention for  
616 each condition is displayed as the percent of GFP positive to total number of inclusions for each  
617 condition.

618

619 ***Effect of ClpX-targeting compounds on chlamydial growth and host cell viability.*** Stocks of  
620 ClpX-specific inhibitor 334 and its derivative, 365, were synthesized as previously reported (44),  
621 resuspended at 25 mg/mL in DMSO, and frozen at -20°C. Methods for the synthesis,  
622 purification, and analysis of these compounds is available in Supplementary Information. A dose  
623 curve of treatment was performed to determine an inhibitory concentration of the compounds on  
624 Ctr, and 25 µg/mL was chosen (data not shown). For the 24 and 48 h samples, 500 µL of DMEM  
625 containing 25 µg/mL of the compounds were added at 8 hpi, and samples were harvested at the  
626 indicated timepoint. For the time of infection samples, compounds were added at 15 minutes  
627 post-infection and removed at 8 hpi. For the reactivation samples, DMEM containing the  
628 respective compound was added at 8 hpi, washed out three times with HBSS at 24 hpi, and then  
629 replaced with DMEM only for 24 additional hours prior to harvest. To determine the effect on  
630 preformed EBs, compound was added at 24 hpi, and samples were harvested at 48 hpi. To  
631 harvest, three wells of a 24-well plate were scraped into 2SP, vortexed with 3 mm glass beads,  
632 and frozen at -80<sup>0</sup> C. Samples were titrated onto a fresh monolayer of HEp2 cells with no  
633 treatment for enumeration.

634

635 **Acknowledgements**

636           We thank Dr. H. Caldwell (NIH/NIAID) for eukaryotic cell lines, Dr. T. Hackstadt  
637 (RML/NIAID) for providing antibodies and the pBOMB4-Tet::*L2* plasmid, Dr. P. Scott Hefty  
638 (KU) for the pTLR2-gfp::*L2* plasmid, and Dr. Peter Sass (University of Tuebingen) for the  
639 BL21(DE3)  $\Delta$ *clpPAX* *E. coli* strain used in this research. This project was supported by a  
640 National Science Foundation CAREER award (1810599) and an NIAID/National Institutes of  
641 Health award (R21AI141933-01) to SPO and by University funds to DJF. This project was also  
642 funded by NIGMS/National Institutes of Health award to the Nebraska Center for Molecular  
643 Target Discovery and Development (1P20GM121316-01A1, PI: Robert Lewis, Project Leader,  
644 MCS).

645

References:

- 646  
647  
648 1. CDC. 2017. 2017 Sexually Transmitted Diseases Surveillance.  
649 <https://www.cdc.gov/std/stats16/chlamydia.htm#foot-1>. Accessed December 2018.  
650 2. WHO. 2018. Trachoma. <http://www.who.int/mediacentre/factsheets/fs382/en/>. Accessed  
651 3. AbdelRahman YM, Belland RJ. 2006. The chlamydial developmental cycle. FEMS  
652 Microbiology Reviews 29:949-959.  
653 4. Hatch TP, Allan I, Pearce JH. 1984. Structural and polypeptide differences between  
654 envelopes of infective and reproductive life cycle forms of *Chlamydia* spp. Journal of  
655 Bacteriology 157:13-20.  
656 5. Hackstadt T, Baehr W, Ying Y. 1991. *Chlamydia trachomatis* developmentally regulated  
657 protein is homologous to eukaryotic histone H1. Proceedings of the National Academy of  
658 Sciences of the United States of America 88:3937-3941.  
659 6. Clifton DR, Fields KA, Grieshaber SS, Dooley CA, Fischer ER, Mead DJ, Carabeo RA,  
660 Hackstadt T. 2004. A chlamydial type III translocated protein is tyrosine-phosphorylated  
661 at the site of entry and associated with recruitment of actin. Proceedings of the National  
662 Academy of Sciences of the United States of America 101:10166.  
663 7. Lane BJ, Mutchler C, Al Khodor S, Grieshaber SS, Carabeo RA. 2008. Chlamydial Entry  
664 Involves TARP Binding of Guanine Nucleotide Exchange Factors. PLoS Pathogens  
665 4:e1000014.  
666 8. Hodinka RL, Davis CH, Choong J, Wyrick PB. 1988. Ultrastructural study of  
667 endocytosis of *Chlamydia trachomatis* by McCoy cells. Infection and Immunity 56:1456-  
668 1463.  
669 9. Moore ER, Ouellette SP. 2014. Reconceptualizing the chlamydial inclusion as a  
670 pathogen-specified parasitic organelle: an expanded role for Inc proteins. Frontiers in  
671 Cellular and Infection Microbiology 4:157.  
672 10. Abdelrahman Y, Ouellette SP, Belland RJ, Cox JV. 2016. Polarized Cell Division of  
673 *Chlamydia trachomatis*. PLoS pathogens 12:e1005822-e1005822.  
674 11. Saka HA, Thompson JW, Chen Y-S, Kumar Y, Dubois LG, Moseley MA, Valdivia RH.  
675 2011. Quantitative proteomics reveals metabolic and pathogenic properties of *Chlamydia*  
676 *trachomatis* developmental forms. Molecular Microbiology 82:1185-1203.  
677 12. Belland RJ, Zhong G, Crane DD, Hogan D, Sturdevant D, Sharma J, Beatty WL,  
678 Caldwell HD. 2003. Genomic transcriptional profiling of the developmental cycle of  
679 *Chlamydia trachomatis*. Proceedings of the National Academy of Sciences of the United  
680 States of America 100:8478-8483.  
681 13. Vandahl BBS, Birkelund S, Christiansen G. 2004. Genome and proteome analysis of  
682 *Chlamydia*. PROTEOMICS 4:2831-2842.  
683 14. Skipp PJS, Hughes C, McKenna T, Edwards R, Langridge J, Thomson NR, Clarke IN.  
684 2016. Quantitative Proteomics of the Infectious and Replicative Forms of *Chlamydia*  
685 *trachomatis*. PLoS ONE 11:e0149011.  
686 15. Higgins D, Dworkin J. 2012. Recent progress in *Bacillus subtilis* sporulation. FEMS  
687 microbiology reviews 36:131-148.  
688 16. Hughes V, Jiang C, Brun Y. 2012. *Caulobacter crescentus*. Current Biology 22:R507-  
689 R509.

- 690 17. Wood NA, Chung K, Blocker A, Rodrigues de Almeida N, Conda-Sheridan M, Fisher  
691 DJ, Ouellette SP. 2018. Initial Characterization of the Two ClpP Paralogs of *Chlamydia*  
692 *trachomatis* Suggests Unique Functionality for Each. *Journal of Bacteriology*.
- 693 18. Stephens RS, Kalman S, Lammel C, Fan J, Marathe R, Aravind L, Mitchell W, Olinger  
694 L, Tatusov RL, Zhao Q, Koonin EV, Davis RW. 1998. Genome Sequence of an Obligate  
695 Intracellular Pathogen of Humans: *Chlamydia trachomatis*. *Science* 282:754.
- 696 19. Singh SK, Grimaud R, Hoskins JR, Wickner S, Maurizi MR. 2000. Unfolding and  
697 internalization of proteins by the ATP-dependent proteases ClpXP and ClpAP.  
698 *Proceedings of the National Academy of Sciences of the United States of America*  
699 97:8898-8903.
- 700 20. Hwang BJ, Park WJ, Chung CH, Goldberg AL. 1987. *Escherichia coli* contains a soluble  
701 ATP-dependent protease (Ti) distinct from protease La. *Proceedings of the National*  
702 *Academy of Sciences of the United States of America* 84:5550-5554.
- 703 21. Walker JE, Saraste M, Runswick MJ, Gay NJ. 1982. Distantly related sequences in the  
704 alpha- and beta-subunits of ATP synthase, myosin, kinases and other ATP-requiring  
705 enzymes and a common nucleotide binding fold. *The EMBO Journal* 1:945-951.
- 706 22. Wendler P, Ciniawsky S, Kock M, Kube S. 2012. Structure and function of the AAA+  
707 nucleotide binding pocket. *Biochimica et Biophysica Acta (BBA) - Molecular Cell*  
708 *Research* 1823:2-14.
- 709 23. Baker TA, Sauer RT. 2012. ClpXP, an ATP-powered unfolding and protein-degradation  
710 machine. *Biochimica et biophysica acta* 1823:15-28.
- 711 24. Wojtyra UA, Thibault G, Tuite A, Houry WA. 2003. The N-terminal Zinc Binding  
712 Domain of ClpX Is a Dimerization Domain That Modulates the Chaperone Function.  
713 *Journal of Biological Chemistry* 278:48981-48990.
- 714 25. Donaldson LW, Wojtyra U, Houry WA. 2003. Solution Structure of the Dimeric Zinc  
715 Binding Domain of the Chaperone ClpX. *Journal of Biological Chemistry* 278:48991-  
716 48996.
- 717 26. Erzberger JP, Berger JM. 2006. Evolutionary relationships and structural mechanisms of  
718 AAA+ proteins. *Annu Rev Biophys Biomol Struct* 35:93-114.
- 719 27. Siddiqui SM, Sauer RT, Baker TA. 2004. Role of the processing pore of the ClpX AAA+  
720 ATPase in the recognition and engagement of specific protein substrates. *Genes &*  
721 *development* 18:369-374.
- 722 28. Martin A, Baker TA, Sauer RT. 2008. Diverse pore loops of the AAA+ ClpX machine  
723 mediate unassisted and adaptor-dependent recognition of *ssrA*-tagged substrates.  
724 *Molecular cell* 29:441-450.
- 725 29. Martin A, Baker TA, Sauer RT. 2008. Pore loops of the AAA+ ClpX machine grip  
726 substrates to drive translocation and unfolding. *Nature structural & molecular biology*  
727 15:1147-1151.
- 728 30. Iosefson O, Olivares AO, Baker TA, Sauer RT. 2015. Dissection of Axial-Pore Loop  
729 Function during Unfolding and Translocation by a AAA+ Proteolytic Machine. *Cell*  
730 *reports* 12:1032-1041.
- 731 31. Iosefson O, Nager AR, Baker TA, Sauer RT. 2015. Coordinated gripping of substrate by  
732 subunits of a AAA+ proteolytic machine. *Nature chemical biology* 11:201-206.
- 733 32. Ogura T, Whiteheart SW, Wilkinson AJ. 2004. Conserved arginine residues implicated in  
734 ATP hydrolysis, nucleotide-sensing, and inter-subunit interactions in AAA and AAA+  
735 ATPases. *Journal of Structural Biology* 146:106-112.



- 736 33. Kim Y-I, Levchenko I, Fraczkowska K, Woodruff RV, Sauer RT, Baker TA. 2001.  
737 Molecular determinants of complex formation between Clp/Hsp100 ATPases and the  
738 ClpP peptidase. *Nature Structural Biology* 8:230.
- 739 34. Amor AJ, Schmitz KR, Baker TA, Sauer RT. 2019. Roles of the ClpX IGF loops in ClpP  
740 association, dissociation, and protein degradation. *Protein Science* 28:756-765.
- 741 35. Brickman TJ, Barry CE, 3rd, Hackstadt T. 1993. Molecular cloning and expression of  
742 *hctB* encoding a strain-variant chlamydial histone-like protein with DNA-binding  
743 activity. *Journal of bacteriology* 175:4274-4281.
- 744 36. Barry Iii CE, Brickman TJ, Hackstadt T. 1993. Hc1-mediated effects on DNA structure: a  
745 potential regulator of chlamydial development. *Molecular Microbiology* 9:273-283.
- 746 37. Fahr MJ, Douglas AL, Xia W, Hatch TP. 1995. Characterization of late gene promoters  
747 of *Chlamydia trachomatis*. *Journal of bacteriology* 177:4252-4260.
- 748 38. Ouellette SP. 2018. Feasibility of a Conditional Knockout System for *Chlamydia* Based  
749 on CRISPR Interference. *Frontiers in Cellular and Infection Microbiology* 8:59.
- 750 39. Ran FA, Cong L, Yan WX, Scott DA, Gootenberg JS, Kriz AJ, Zetsche B, Shalem O, Wu  
751 X, Makarova KS, Koonin EV, Sharp PA, Zhang F. 2015. *In vivo* genome editing using  
752 *Staphylococcus aureus* Cas9. *Nature* 520:186-191.
- 753 40. Suchland RJ, Rockey DD, Bannantine JP, Stamm WE. 2000. Isolates of *Chlamydia*  
754 *trachomatis* That Occupy Nonfusogenic Inclusions Lack IncaA, a Protein Localized to the  
755 Inclusion Membrane. *Infection and Immunity* 68:360.
- 756 41. Wichlan DG, Hatch TP. 1993. Identification of an early-stage gene of *Chlamydia psittaci*  
757 6BC. *Journal of Bacteriology* 175:2936-2942.
- 758 42. Shaw EI, Dooley CA, Fischer ER, Scidmore MA, Fields KA, Hackstadt T. 2002. Three  
759 temporal classes of gene expression during the *Chlamydia trachomatis* developmental  
760 cycle. *Molecular Microbiology* 37:913-925.
- 761 43. Johnson FWA, Hobson D. 1977. The effect of penicillin on genital strains of *Chlamydia*  
762 *trachomatis* in tissue culture. *Journal of Antimicrobial Chemotherapy* 3:49-56.
- 763 44. Fetzer C, Korotkov VS, Thänert R, Lee KM, Neuenschwander M, von Kries JP, Medina  
764 E, Sieber SA. 2017. A Chemical Disruptor of the ClpX Chaperone Complex Attenuates  
765 the Virulence of Multidrug-Resistant *Staphylococcus aureus*. *Angewandte Chemie*  
766 *International Edition* 56:15746-15750.
- 767 45. Trott O, Olson AJ. 2010. AutoDock Vina: improving the speed and accuracy of docking  
768 with a new scoring function, efficient optimization, and multithreading. *Journal of*  
769 *computational chemistry* 31:455-461.
- 770 46. Olivares AO, Baker TA, Sauer RT. 2016. Mechanistic insights into bacterial AAA+  
771 proteases and protein-remodelling machines. *Nature reviews Microbiology* 14:33-44.
- 772 47. Martin A, Baker TA, Sauer RT. 2007. Distinct static and dynamic interactions control  
773 ATPase-peptidase communication in a AAA+ protease. *Molecular cell* 27:41-52.
- 774 48. Singh SK, Rozycki J, Ortega J, Ishikawa T, Lo J, Steven AC, Maurizi MR. 2001.  
775 Functional Domains of the ClpA and ClpX Molecular Chaperones Identified by Limited  
776 Proteolysis and Deletion Analysis. *Journal of Biological Chemistry* 276:29420-29429.
- 777 49. Thomson NR, Holden MTG, Carder C, Lennard N, Lockey SJ, Marsh P, Skipp P,  
778 O'Connor CD, Goodhead I, Norbertzcak H, Harris B, Ormond D, Rance R, Quail MA,  
779 Parkhill J, Stephens RS, Clarke IN. 2008. *Chlamydia trachomatis*: genome sequence  
780 analysis of lymphogranuloma venereum isolates. *Genome research* 18:161-171.

- 781 50. Moore SD, Sauer RT. 2007. The tmRNA System for Translational Surveillance and  
782 Ribosome Rescue. *Annual Review of Biochemistry* 76:101-124.
- 783 51. Moore SD, Sauer RT. 2005. Ribosome rescue: tmRNA tagging activity and capacity in  
784 *Escherichia coli*. *Molecular Microbiology* 58:456-466.
- 785 52. Hudson CM, Williams KP. 2014. The tmRNA website. *Nucleic Acids Research*  
786 43:D138-D140.
- 787 53. Abo T, Inada T, Ogawa K, Aiba H. 2000. SsrA-mediated tagging and proteolysis of LacI  
788 and its role in the regulation of *lac* operon. *The EMBO Journal* 19:3762.
- 789 54. Dulebohn D, Choy J, Sundermeier T, Okan N, Karzai AW. 2007. Trans-Translation: The  
790 tmRNA-Mediated Surveillance Mechanism for Ribosome Rescue, Directed Protein  
791 Degradation, and Nonstop mRNA Decay. *Biochemistry* 46:4681-4693.
- 792 55. Pan S, Malik IT, Thomy D, Henrichfreise B, Sass P. 2019. The functional ClpXP  
793 protease of *Chlamydia trachomatis* requires distinct clpP genes from separate genetic  
794 loci. *Scientific Reports* 9:14129.
- 795 56. Zhang Y, Zuber P. 2007. Requirement of the zinc-binding domain of ClpX for Spx  
796 proteolysis in *Bacillus subtilis* and effects of disulfide stress on ClpXP activity. *Journal of*  
797 *bacteriology* 189:7669-7680.
- 798 57. Park EY, Lee B-G, Hong S-B, Kim H-W, Jeon H, Song HK. 2007. Structural Basis of  
799 SspB-tail Recognition by the Zinc Binding Domain of ClpX. *Journal of Molecular*  
800 *Biology* 367:514-526.
- 801 58. Howard MB, Ekborg NA, Taylor LE, Hutcheson SW, Weiner RM. 2004. Identification  
802 and analysis of polyserine linker domains in prokaryotic proteins with emphasis on the  
803 marine bacterium *Microbulbifer degradans*. *Protein science : a publication of the Protein*  
804 *Society* 13:1422-1425.
- 805 59. Shen H, Schmuck M, Pilz I, Gilkes NR, Kilburn DG, Miller RC, Warren RA. 1991.  
806 Deletion of the linker connecting the catalytic and cellulose-binding domains of  
807 endoglucanase A (CenA) of *Cellulomonas fimi* alters its conformation and catalytic  
808 activity. *Journal of Biological Chemistry* 266:11335-11340.
- 809 60. Gatsogiannis C, Balogh D, Merino F, Sieber SA, Raunser S. 2019. Cryo-EM structure of  
810 the ClpXP protein degradation machinery. *Nature Structural & Molecular Biology*  
811 26:946-954.
- 812 61. Song B, Bomar MG, Kibler P, Kodukula K, Galande AK. 2012. The Serine-Proline Turn:  
813 A Novel Hydrogen-Bonded Template for Designing Peptidomimetics. *Organic Letters*  
814 14:732-735.
- 815 62. Hutchinson EG, Thornton JM. 1994. A revised set of potentials for beta-turn formation in  
816 proteins. *Protein science : a publication of the Protein Society* 3:2207-2216.
- 817 63. Matsumoto A, Manire GP. 1970. Electron Microscopic Observations on the Effects of  
818 Penicillin on the Morphology of *Chlamydia psittaci*. *Journal of Bacteriology* 101:278-  
819 285.
- 820 64. Skilton RJ, Cutcliffen LT, Barlow D, Wang Y, Salim O, Lambden PR, Clarke IN. 2009.  
821 Penicillin induced persistence in *Chlamydia trachomatis*: high quality time lapse video  
822 analysis of the developmental cycle. *PloS one* 4:e7723-e7723.
- 823 65. Ouellette SP, Karimova G, Subtil A, Ladant D. 2012. *Chlamydia* co-opts the rod shape-  
824 determining proteins MreB and Pbp2 for cell division. *Molecular Microbiology* 85:164-  
825 178.

- 826 66. Wang Y, Kahane S, Cutcliffe LT, Skilton RJ, Lambden PR, Clarke IN. 2011.  
827 Development of a Transformation System for *Chlamydia trachomatis*: Restoration of  
828 Glycogen Biosynthesis by Acquisition of a Plasmid Shuttle Vector. PLoS Pathogens  
829 7:e1002258.
- 830 67. Kanehisa M, Sato Y, Kawashima M, Furumichi M, Tanabe M. 2016. KEGG as a  
831 reference resource for gene and protein annotation. Nucleic Acids Research 44:D457-  
832 D462.
- 833 68. Kanehisa M, Goto S. 2000. KEGG: Kyoto Encyclopedia of Genes and Genomes. Nucleic  
834 Acids Research 28:27-30.
- 835 69. Kanehisa M, Furumichi M, Tanabe M, Sato Y, Morishima K. 2017. KEGG: new  
836 perspectives on genomes, pathways, diseases and drugs. Nucleic Acids Research  
837 45:D353-D361.
- 838 70. Altschul SF, Wootton JC, Gertz EM, Agarwala R, Morgulis A, Schäffer AA, Yu Y-K.  
839 2005. Protein Database Searches Using Compositionally Adjusted Substitution Matrices.  
840 The FEBS journal 272:5101-5109.
- 841 71. Sievers F, Wilm A, Dineen D, Gibson TJ, Karplus K, Li W, Lopez R, McWilliam H,  
842 Remmert M, Söding J, Thompson JD, Higgins DG. 2011. Fast, scalable generation of  
843 high-quality protein multiple sequence alignments using Clustal Omega. Molecular  
844 Systems Biology 7:539-539.
- 845 72. Troshin PV, Procter JB, Barton GJ. 2011. Java bioinformatics analysis web services for  
846 multiple sequence alignment—JABAWS:MSA. Bioinformatics 27:2001-2002.
- 847 73. Kelley LA, Mezulis S, Yates CM, Wass MN, Sternberg MJE. 2015. The Phyre2 web  
848 portal for protein modelling, prediction and analysis. Nature protocols 10:845-858.
- 849 74. Waterhouse A, Rempfer C, Heer FT, Studer G, Tauriello G, Bordoli L, Bertoni M,  
850 Gumienny R, Lepore R, Bienert S, de Beer TA P, Schwede T. 2018. SWISS-MODEL:  
851 homology modelling of protein structures and complexes. Nucleic Acids Research  
852 46:W296-W303.
- 853 75. Waterhouse A, Studer G, Tauriello G, Bordoli L, Bienert S, de Beer Tjaart AP, Schwede  
854 T. 2016. The SWISS-MODEL Repository—new features and functionality. Nucleic  
855 Acids Research 45:D313-D319.
- 856 76. Guex N, Peitsch MC, Schwede T. 2009. Automated comparative protein structure  
857 modeling with SWISS-MODEL and Swiss-PdbViewer: A historical perspective.  
858 ELECTROPHORESIS 30:S162-S173.
- 859 77. Bertoni M, Kiefer F, Biasini M, Bordoli L, Schwede T. 2017. Modeling protein  
860 quaternary structure of homo- and hetero-oligomers beyond binary interactions by  
861 homology. Scientific Reports 7:10480.
- 862 78. Pettersen EF, Goddard TD, Huang CC, Couch GS, Greenblatt DM, Meng EC, Ferrin TE.  
863 2004. UCSF Chimera—A visualization system for exploratory research and analysis.  
864 Journal of Computational Chemistry 25:1605-1612.
- 865 79. Dunbrack RL. 2002. Rotamer Libraries in the 21st Century. Current Opinion in Structural  
866 Biology 12:431-440.
- 867 80. Dunbrack Jr RL, Cohen FE. 1997. Bayesian statistical analysis of protein side-chain  
868 rotamer preferences. Protein Science 6:1661-1681.
- 869 81. Wang J, Wang W, Kollman PA, Case DA. 2006. Automatic atom type and bond type  
870 perception in molecular mechanical calculations. Journal of Molecular Graphics and  
871 Modelling 25:247-260.

- 872 82. Ouellette SP, Gauliard E, Antosová Z, Ladant D. 2014. A Gateway®-compatible  
873 bacterial adenylate cyclase-based two-hybrid system. *Environmental Microbiology*  
874 *Reports* 6:259-267.
- 875 83. Wickstrum J, Sammons LR, Restivo KN, Hefty PS. 2013. Conditional Gene Expression  
876 in *Chlamydia trachomatis* Using the Tet System. *PLoS ONE* 8:e76743.
- 877 84. Bauler LD, Hackstadt T. 2014. Expression and targeting of secreted proteins from  
878 *Chlamydia trachomatis*. *Journal of bacteriology* 196:1325-1334.
- 879 85. Ouellette SP, Hatch TP, AbdelRahman YM, Rose LA, Belland RJ, Byrne GI. 2006.  
880 Global transcriptional upregulation in the absence of increased translation in *Chlamydia*  
881 during IFN $\gamma$ -mediated host cell tryptophan starvation. *Molecular Microbiology* 62:1387-  
882 1401.
- 883 86. Karimova G, Pidoux J, Ullmann A, Ladant D. 1998. A bacterial two-hybrid system based  
884 on a reconstituted signal transduction pathway. *Proceedings of the National Academy of*  
885 *Sciences of the United States of America* 95:5752-5756.
- 886 87. Robichon C, Karimova G, Beckwith J, Ladant D. 2011. Role of Leucine Zipper Motifs in  
887 Association of the *Escherichia coli* Cell Division Proteins FtsL and FtsB. *Journal of*  
888 *Bacteriology* 193:4988-4992.
- 889 88. Mueller KE, Wolf K, Fields KA. 2017. *Chlamydia trachomatis* Transformation and  
890 Allelic Exchange Mutagenesis. *Current Protocols in Microbiology* 45:11A.3.1-11A.3.15.
- 891 89. Schindelin J, Arganda-Carreras I, Frise E, Kaynig V, Longair M, Pietzsch T, Preibisch S,  
892 Rueden C, Saalfeld S, Schmid B, Tinevez J-Y, White DJ, Hartenstein V, Eliceiri K,  
893 Tomancak P, Cardona A. 2012. Fiji: an open-source platform for biological-image  
894 analysis. *Nature methods* 9:676-682.
- 895 90. Ouellette SP, Abdelrahman YM, Belland RJ, Byrne GI. 2005. The *Chlamydia*  
896 *pneumoniae* type III secretion-related lcrH gene clusters are developmentally expressed  
897 operons. *Journal of bacteriology* 187:7853-7856.
- 898 91. Ouellette SP, Rueden KJ, Gauliard E, Persons L, de Boer PA, Ladant D. 2014. Analysis  
899 of MreB interactors in *Chlamydia* reveals a RodZ homolog but fails to detect an  
900 interaction with MraY. *Frontiers in Microbiology* 5:279.
- 901 92. Ouellette SP, Rueden KJ, Rucks EA. 2016. Tryptophan Codon-Dependent Transcription  
902 in *Chlamydia pneumoniae* during Gamma Interferon-Mediated Tryptophan Limitation.  
903 *Infection and Immunity* 84:2703-2713.
- 904

905

906 **Figure Legends**

907 **Figure 1: Bioinformatic analysis of chlamydial ClpX supports its role as a AAA+ ATPase.**

908 **(A) Multiple sequence alignment** of chlamydial ClpX with the ClpX orthologs of various other  
909 bacteria. Ec = *Escherichia coli*, Ctr = *Chlamydia trachomatis*, Bs = *Bacillus subtilis*, Mtb =  
910 *Mycobacterium tuberculosis*, Pa = *Pseudomonas aeruginosa*, Sa = *Staphylococcus aureus*.  
911 Alignment was performed using Clustal Omega with default settings and presented using Jalview  
912 version 2. Alignment was colored by % identity in shades of blue or as indicated below the  
913 alignment. **(B) 3D model** of ClpX was generated using SwissModel and presented in UCSF  
914 Chimera. Conserved motifs pseudo-colored as above in the MSA except the IGF loops, which  
915 are colored lime green. Two subunits of the hexamer were hidden for easier visualization into the  
916 complex. Top and bottom are representations following a 90° either clockwise or  
917 counterclockwise around the X axis. Of note, this model was generated using an ADP-bound  
918 form of ClpX as a template.

919

920 **Figure 2: ClpX is a functional ATPase that forms the expected hexamer. (A) Native-PAGE**

921 **assay** of recombinant ClpX and ClpX<sub>(E187A)</sub>. Expected hexameric size is approximately 283 kDa.

922 **(B) ATP hydrolysis** end point assay using Biomol Green. Levels of detected phosphate are  
923 displayed on the Y axis. Error bars represent standard error and differences between samples are  
924 significant ( $p < 0.05$ , one-way anova). **(C) Bacterial Adenylate Cyclase Two Hybrid**

925 **(BACTH)** assays showing pairwise, homotypic interaction of ClpX and ClpX<sub>(E187A)</sub> as well as  
926 heterotypic interaction of ClpX and ClpX<sub>(E187A)</sub>. **(D)  $\beta$ -Galactosidase activity** of the BACTH  
927 interactions from (C), displayed in arbitrary units on the Y axis.

928

929 **Figure 3: Inactive Clp mutant overexpression negatively impacts Ctr at later timepoints.**

930 **(A) Immunofluorescence assay (IFA) of ClpP2 and ClpX** wild-type and inactive mutant  
931 overexpression at 24 and 48 hpi. Samples induced with 10 nM aTc at 10 hpi. Samples stained for  
932 MOMP (green), 6xHis (red), and DNA (blue). Scale bar = 10  $\mu$ m. Images acquired on a Zeiss  
933 Apotome at 100x magnification. **(B-C) Recoverable inclusion forming units (IFUs)** of wild-  
934 type and mutant ClpP2 (B) or ClpX (C). Samples induced with 10 nM aTc at 10 hpi. IFUs  
935 recovered displayed as Log<sub>10</sub>. Values represent the average of two independent experiments. **(D)**  
936 **IFA of ClpP2X** wild-type or inactive mutant operons at 24 and 48 hpi. Samples stained for  
937 MOMP (pink), FLAG (ClpP2, red), 6xHis (ClpX, green), and DNA (blue). Parameters as  
938 described in previous figure. **(E) IFU recovery assays** of ClpP2X wild-type and mutant  
939 overexpression. IFUs recovered displayed as Log<sub>10</sub>.

940

941 **Figure 4: Functional disruption of ClpX and ClpP2 perturbs chlamydial development, but**

942 **likely in different manners. (A) Fold changes** of detectable gDNA from 24 to 48 hpi for each  
943 strain. Samples induced at 10 hpi with 10 nM aTc. \* =  $p \leq 0.05$ , \*\* =  $p \leq 0.001$  by paired t-test.  
944 Values displayed as the average of three independent experiments with error bars representing  
945 standard deviation. **(B) Western blot** analysis of HctB levels at 48 hpi with and without  
946 overexpression. One well of a six well plate was lysed into 500  $\mu$ L of denaturing lysis buffer. 50  
947  $\mu$ g of protein from the clarified lysate for each sample was loaded and run. Blots were probed for  
948 MOMP (IR680) and HctB (IR800). Grayscale blot shown is representative of three independent  
949 experiments. **(C) Quantified integrated** density of the staining from (B). HctB levels were  
950 normalized to MOMP levels in each sample to account for differences in bacteria in each sample.

951 Values displayed as levels of induced to uninduced HctB/MOMP ratios for each strain. \* =  $p \leq$   
952 0.05, \*\* =  $p \leq 0.001$ , ns = not significant by multiple comparisons t-test.

953

954 **Figure 5: Knockdown of *clpP2X* expression negatively impacts *Chlamydia*.** (A) **Transcript**  
955 **levels** upon knockdown of *clpP2X* by CRISPR interference. Data displayed are the average and  
956 standard deviation of three independent biological replicates of triplicate RT-qPCR reactions.  
957 Values are normalized to the 10h uninduced ClpP2 value for each experiment. Samples were  
958 induced using 10 nM aTc. (B) **Immunofluorescence staining** to confirm knockdown of IncA  
959 upon induction of dCas9 expression. Sa\_dCas9 was induced or not at 4 hpi. Samples were  
960 harvested at 24 hpi and were stained for chlamydial MOMP (green), IncA (magenta), and DNA  
961 (Blue). Scale bar = 10  $\mu\text{m}$ . (C) **Recoverable inclusion forming units (IFUs)** following  
962 induction of knockdown at 4 hpi. Values are presented on a  $\text{Log}_{10}$  scale percent of the respective  
963 uninduced titer. Error bars represent standard deviation between experiments. (D) **Plasmid**  
964 **retention** based on the ratio of GFP positive to total number of inclusions is displayed in percent  
965 for each condition. Error bars represent the standard deviations of three independent biological  
966 replicates.

967

968 **Figure 6: Chemical disruption of ClpX function is highly detrimental to *Chlamydia*.** (A)  
969 **Immunofluorescence assay (IFA)** of 24 hours post-infection (hpi). All drugs added at a final  
970 concentration of 25  $\mu\text{g}/\text{mL}$ . Drugs were added at 8 hpi for the 24 h treatment samples. Drugs  
971 were added 15 minutes post-infection and removed at 8 hpi for the TOI: 8 h pulse samples.  
972 MOMP is stained in green, and DNA is stained with DAPI. Images were acquired on a Zeiss  
973 LSM800 microscope at 63x magnification. Scale bar = 10  $\mu\text{m}$ . TOI = Time of Infection. (B) **IFA**

974 **of 48 hpi** samples. Samples stained for MOMP (green) and DNA (blue). Scale bar = 10  $\mu\text{m}$ .  
975 Drug was added at 8 hpi for 48 h and reactivation samples. Media removed, drug washed out,  
976 and media with drug added back to +Drug at 24 h and 48 h samples. Reactivation samples media  
977 replaced with DMEM, no drug. **(C) Recoverable inclusion forming units (IFUs)** from the  
978 indicated conditions. Totals present as  $\text{Log}_{10}$  IFUs recovered. Standard deviation displayed on  
979 graphs as error bars.

980

### 981 **Supplemental Figure Legends**

982 **Figure S1: Transmission electron microscopy of inactive Clp overexpression. (A)**  
983 **Representative ClpP<sub>2S98A</sub> uninduced or induced** samples at 48 hpi. Samples were induced or  
984 not with 10 nM aTc at 10 hpi and were fixed and processed at 48 hpi. Arrows indicate abnormal  
985 forms in the induced samples. Scale bar = 2  $\mu\text{m}$ . **(B) Representative ClpX<sub>E187A</sub> uninduced or**  
986 **induced** samples at 48 hpi. Samples treated, fixed, and processed as previously discussed.  
987 Arrows indicate abnormal forms with intrabacterial aggregates. Scale bar = 2  $\mu\text{m}$ . **(C and D)**  
988 **Zoomed images of boxed regions from ClpX<sub>E187A</sub> uninduced** samples at 48hpi.

989

990 **Figure S2: RT-qPCR of *clpP1*, *euo*, and *omcB* upon *clpP2X* knockdown.** Data shown are the  
991 average of three biological replicates, each with three technical replicates. Values are normalized  
992 to the 10h timepoint for each respective gene. Error bars represent standard deviation. Samples  
993 induced as indicated with 10 nM aTc.

994

995 **Figure S3: Docking simulation of the ClpX inhibitor 334 on a ClpX model. (A) PDB**  
996 **structure** of 334. Inset is the 2D structure of the drug. **(B) Ribbon model** of docked 334 within



997 the ClpX hexamer. The best scoring model is shown. Only the two ClpX subunits making  
998 contact with the model are shown (A in gray, B in seafoam green). The Walker A motif (red),  
999 Walker B motif (purple), sensor 1 motif (dark green), and sensor 2 motif (orange) of subunit A  
1000 are colored for visualization. The arginine finger is labeled light green of subunit B. The center  
1001 picture is oriented as outside of the complex looking inward, and the other images are rotations  
1002 as indicated. **(C) Surface rendering** of the ClpX subunits with docked 334 are shown with  
1003 coloration as in (B).

1004  
1005 **Figure S4: Docking simulation of the ClpX inhibitor 365 on a ClpX model. (A) PDB**  
1006 **structure** of 365. Inset is the 2D structure of the drug. **(B) Ribbon model** of docked 365 within  
1007 the ClpX hexamer. The best scoring model is shown. Only the two ClpX subunits making  
1008 contact with the model are shown (A in gray, B in seafoam green). The Walker A motif (red),  
1009 Walker B motif (purple), sensor 1 motif (dark green), and sensor 2 motif (orange) of subunit A  
1010 are colored for visualization. The arginine finger is labeled light green of subunit B. The center  
1011 picture is oriented as outside of the complex looking inward, and the other images are rotations  
1012 as indicated. **(C) Surface rendering** of the ClpX subunits with docked 365 are shown with  
1013 coloration as in (B).

1014  
1015 **Figure S5: Proposed model for ClpP2X function in *Chlamydia*.** An RB ultimately has two  
1016 fates: differentiation or replication. Based on our data showing the impact of ClpP2 disruption on  
1017 the developmental cycle, we hypothesize that ClpP2 may play a role in triggering either event  
1018 based on its degradative target at either timepoint. Furthermore, we posit that ClpX may play a

1019 substantial role in EB organization, given that ClpX affects recoverable IFUs without reducing  
1020 the amount of HctB produced.

1021

1022 **Figure S6. Example ClpX protein purifications.** Recombinant, 6x His-tagged  
1023 ClpX/ClpX<sub>(E187A)</sub> were purified using cobalt-based immobilized metal affinity chromatography.  
1024 Samples were quantified and 1 and 5 µg aliquots were run on 10% SDS-PAGE followed by  
1025 staining with Coomassie brilliant blue. Three ClpX and two ClpX<sub>(E187A)</sub> purification were  
1026 performed using BL21(DE3)  $\Delta clpPAX$  *E. coli*.

1027

1028 **Supplemental Table 1.** List of primers, plasmids, and strains used in this study.

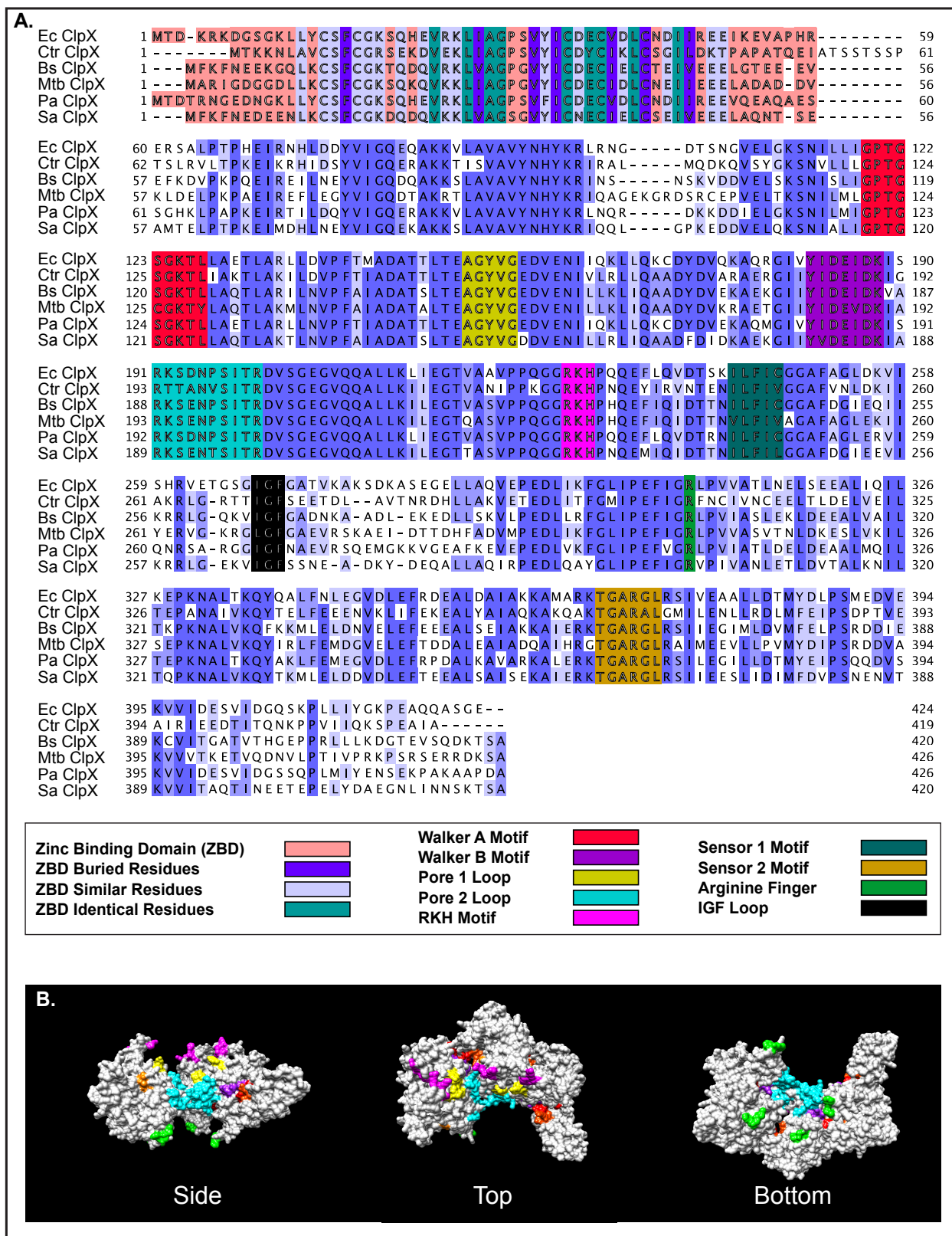
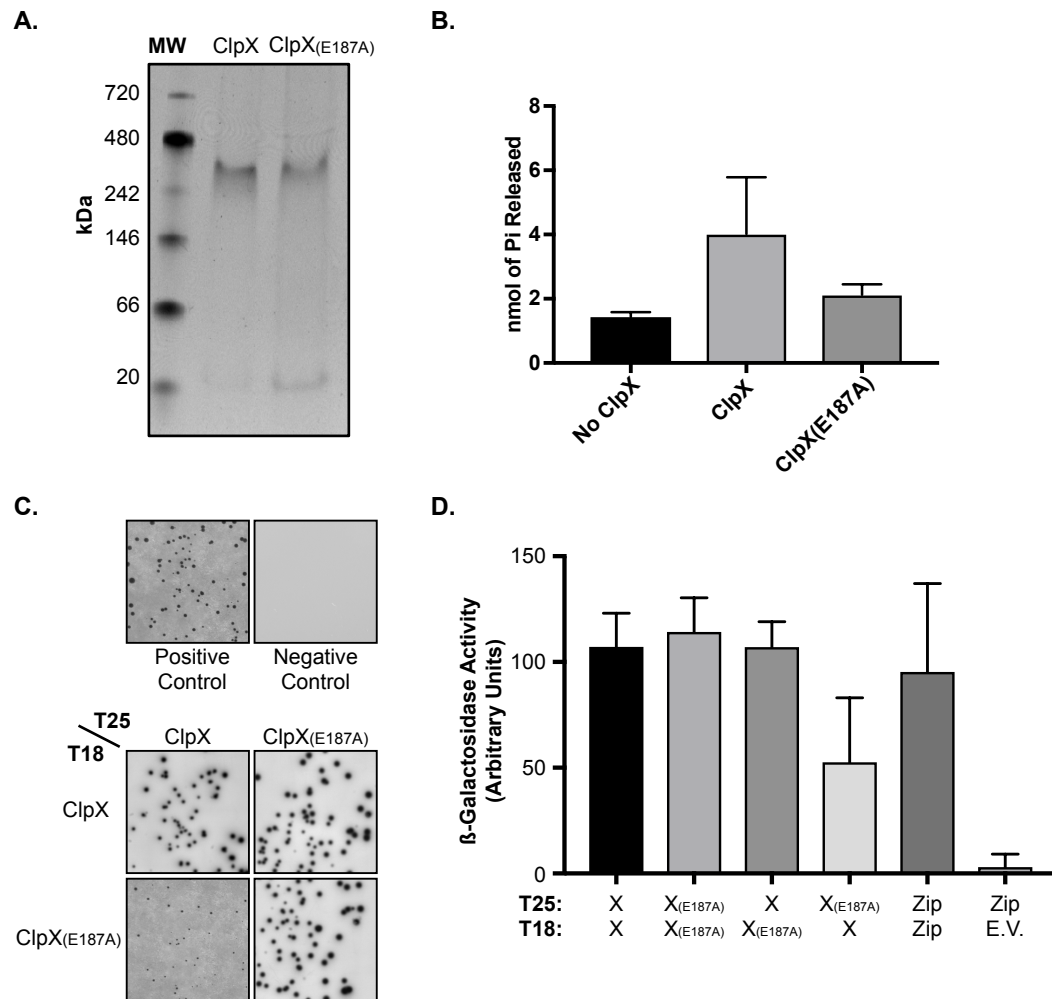
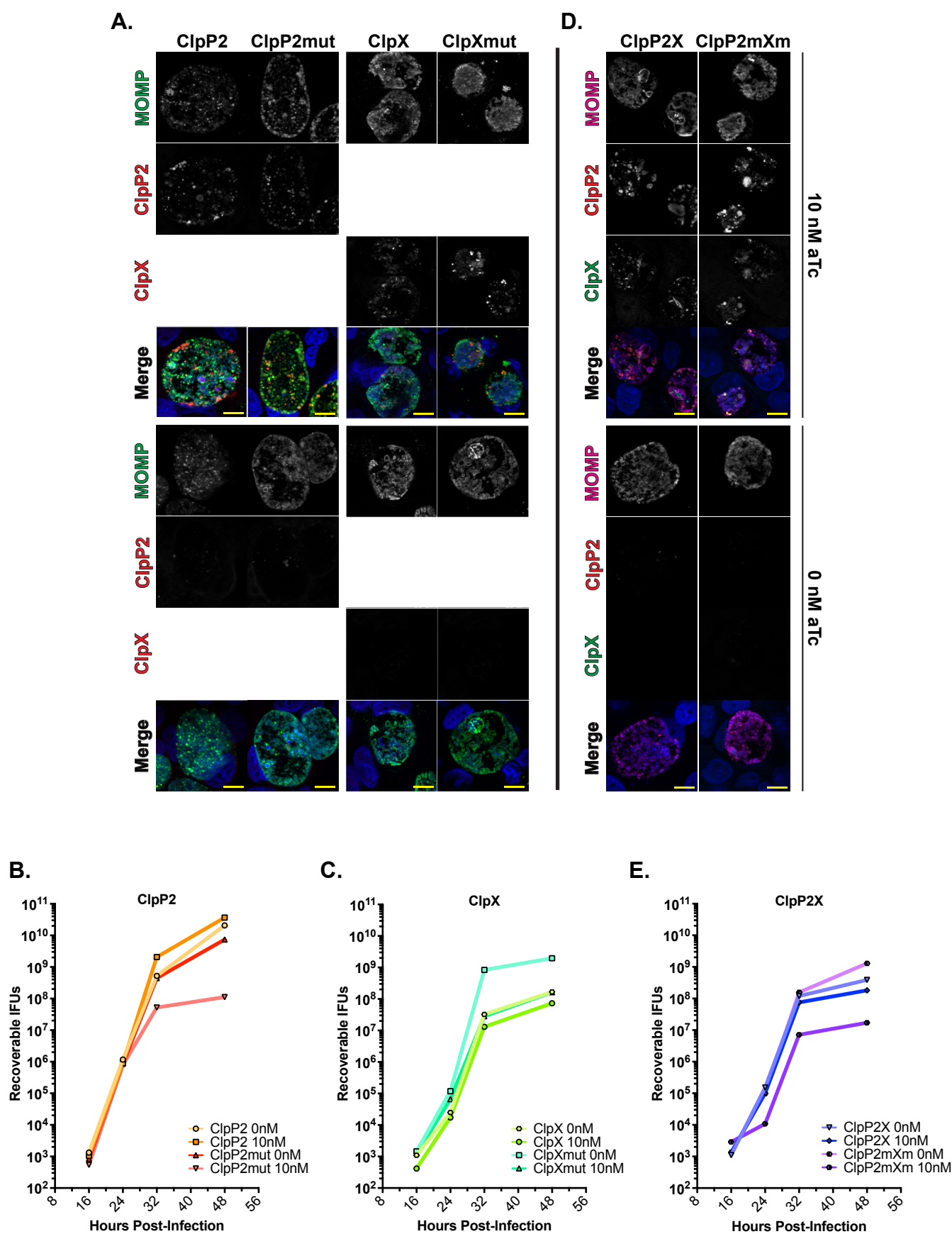


Fig. 1



**Fig. 2**



**Fig. 3**

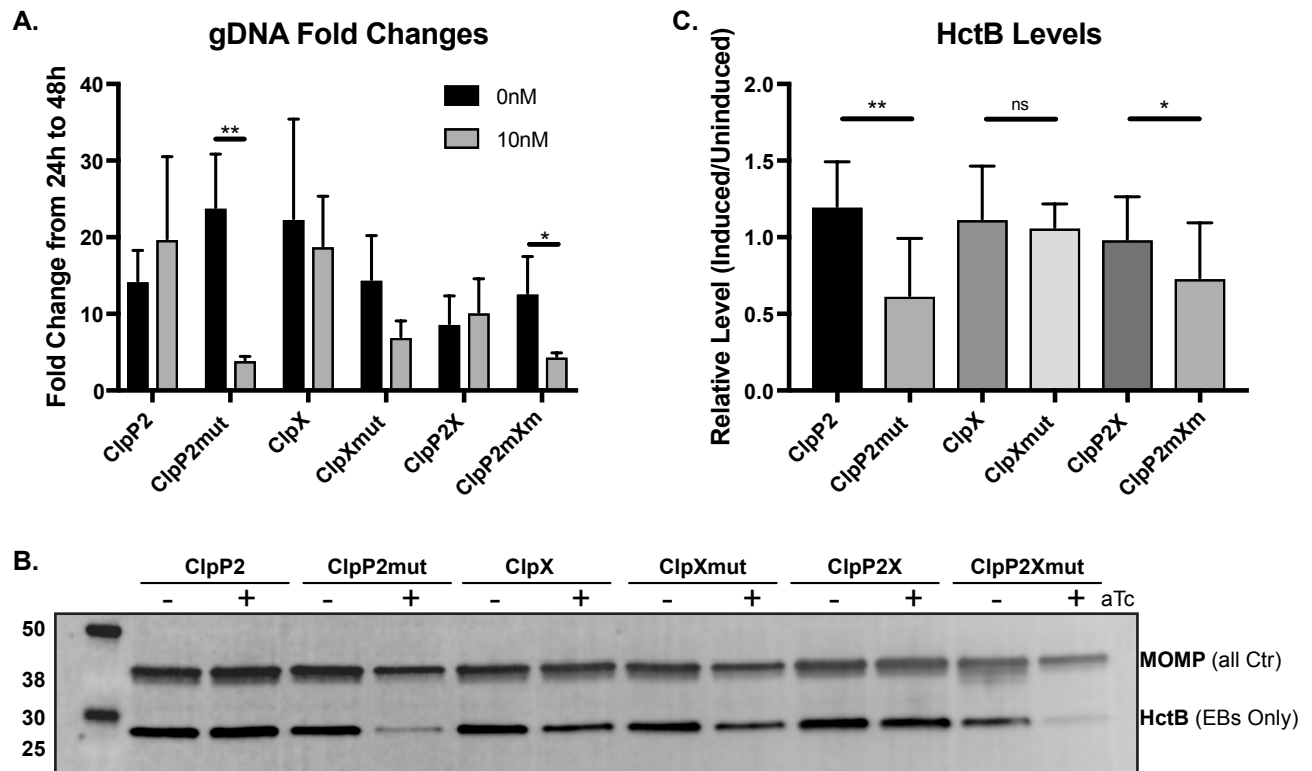


**Fig. 4**

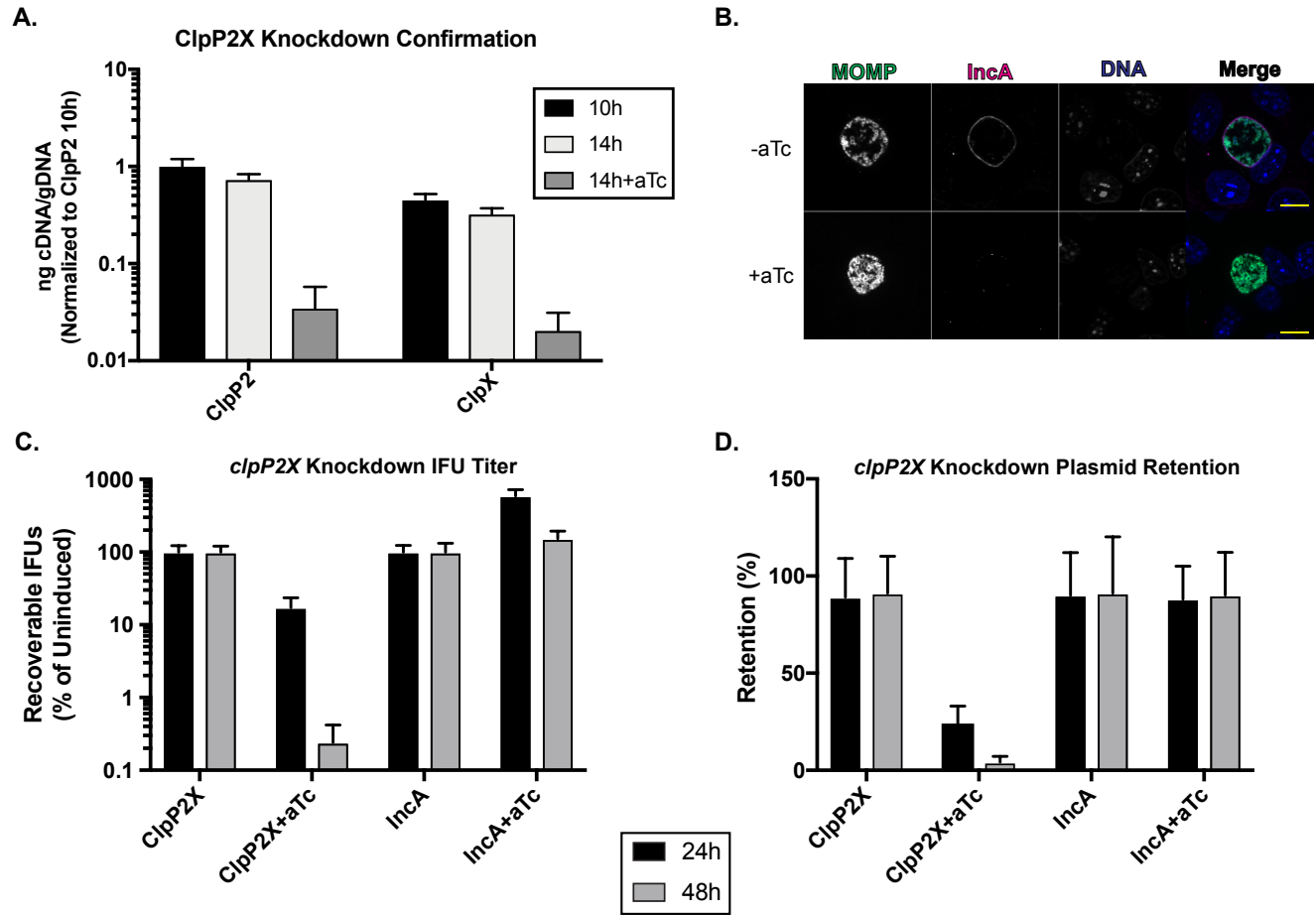


**Fig. 5**

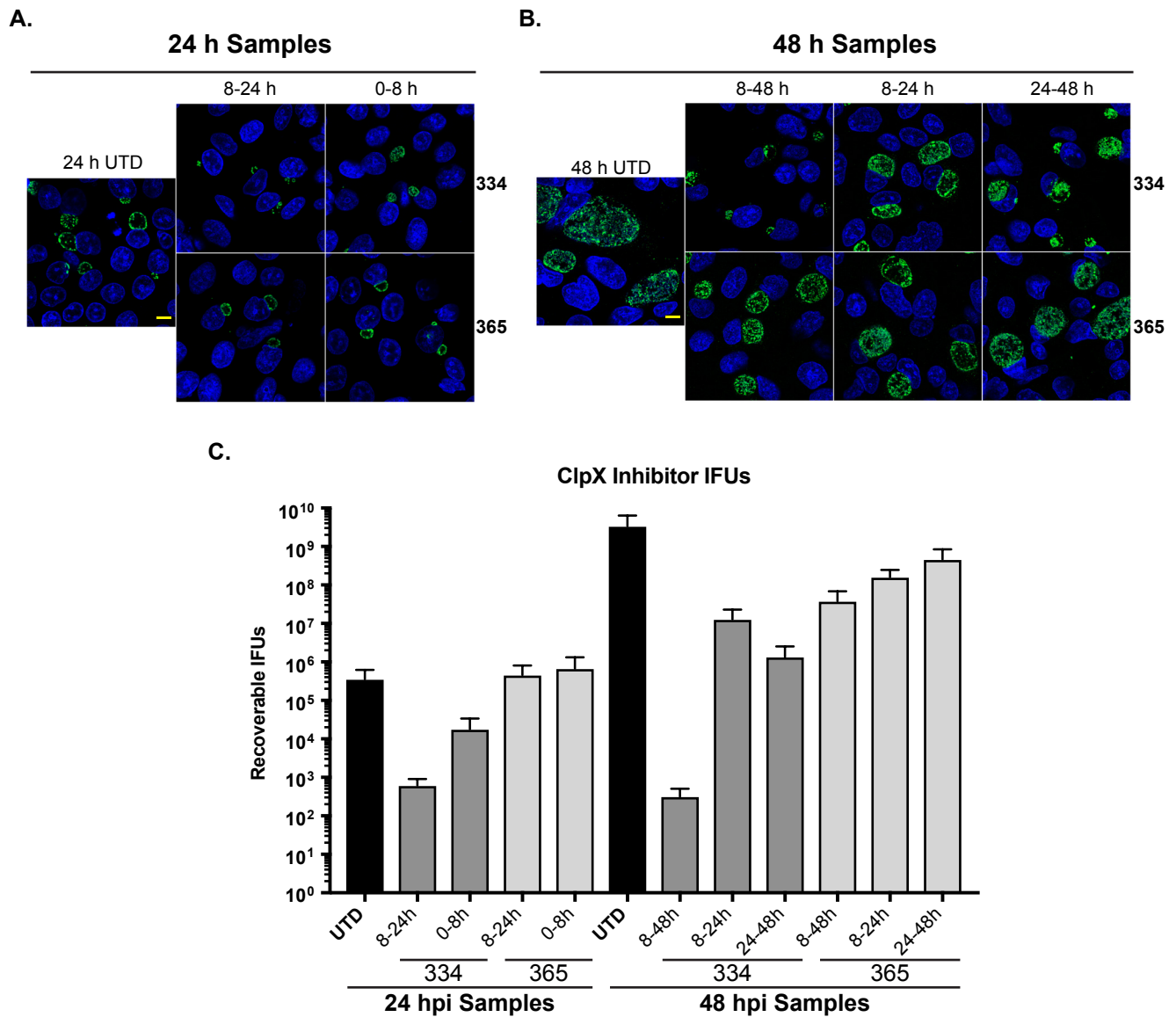


**Fig. 6**